

学位論文

Ab initio quantum Monte Carlo study on hydrogen impurities in silica

(第一原理量子モンテカルロ法によるシリカ中の
水素不純物に関する研究)

平成 27 年 12 月 博士 (理学) 申請

東京大学大学院理学系研究科
物理学専攻

山本 良幸

Abstract

The hydrogen impurity is ubiquitous in all semiconductors. Hydrogen unavoidably penetrates into samples in many growth techniques and changes their electronic and optical properties. In solids, hydrogen impurity can take several charge and bonding states, and this is the origin of the wide variety of phenomena caused by hydrogen. Because experimental detection of hydrogen impurity is rather challenging, theoretical study is essential to understand the properties of hydrogen impurity.

In this thesis, we performed a reliable simulation of hydrogen impurity in silica based on first-principles methods. To describe electronic structures, we used the diffusion Monte Carlo (DMC) method, which is known to be one of the most reliable methods to simulate electronic systems in condensed matter. Furthermore, we developed a method to calculate the transition barriers between different charge states by extending the nudged elastic band (NEB) method.

We calculated the formation energy of three possible charge states of hydrogen (H^- , H^0 and H^+) in quartz SiO_2 ($q\text{-SiO}_2$) and rutile SiO_2 ($r\text{-SiO}_2$) with density functional theory (DFT) and DMC. Atomic configurations optimized with generalized-gradient approximations (GGA) within DFT are used also for DMC. The finite-size effects of charged states are corrected with the Makov-Payne (MP) correction. Compared to DFT, the calculated formation energy with DMC are lower for H^+ in $q\text{-SiO}_2$ and higher for H^- in $r\text{-SiO}_2$, while the calculated formation energy of H^0 is larger than that of H^- and H^+ in all the range of electron chemical potential with both DFT and DMC. Hence we conclude that the H^0 state is thermodynamically unstable in the both polymorphs of SiO_2 , and this is consistent with electron spin resonance experiments.

Transition barriers between different charge states of hydrogen impurities in silica were estimated with simple linear interpolated paths and optimized paths calculated with the extended NEB method. Calculated transition barriers with the extended NEB method are several tenth of an eV lower than that with the straight path. The transition barrier calculated with DMC is larger than that with DFT both for $q\text{-SiO}_2$ and $r\text{-SiO}_2$. Each charge state has a finite transition barrier in some regions of the electron chemical potential. Experimental detections of large amount of muonium, which is a small-mass counterpart

of H^0 , is explained by its metastability that has finite transition barriers to other states.

Finally, we studied possible molecular complexes of two hydrogen impurities. For q - SiO_2 , we found two stable complexes, H_2 molecule and H_2^* . The latter is a complex of nearest-neighbored H^+ and H^- impurities. As a two hydrogen complex, only $\text{H}^+ + \text{H}^+$ and H_2 and $\text{H}^- + \text{H}^-$ are thermodynamically stable in q - SiO_2 . For r - SiO_2 , we found two stable complexes, H_2 molecule and H_2^+ molecule. H_2^+ molecule is uniquely found in r - SiO_2 . The calculated formation energies indicate that thermodynamically stable complexes are H_2 and $\text{H}^+ + \text{H}^+$. Thermodynamically stable states are common to DFT and DMC.

This thesis reveals the thermodynamic and metastable properties of hydrogen impurities in silica with the state-of-the-art first-principles methods.

Contents

1	Introduction	7
1.1	Hydrogen impurity in semiconductors	7
1.2	Hydrogen impurity in silica: previous studies	9
1.3	Purposes and outline of this study	11
2	Density functional theory and quantum Monte Carlo method	15
2.1	Density functional theory	15
2.2	Quantum Monte Carlo method	16
2.2.1	Variational Monte Carlo method	17
2.2.2	Diffusion Monte Carlo method	18
2.3	Defective system	19
2.3.1	Charge state calculation	19
2.3.2	Formation energy	20
3	Nudged elastic band method for transition barriers between different charge states	23
3.1	Nudged elastic band method	23
3.2	Extended nudged elastic band method	25
4	Isolated hydrogen atom in silica	27
4.1	Computational details	27
4.1.1	Density functional theory	27
4.1.2	Diffusion Monte Carlo method	28
4.2	Relaxed structures and density of states	30
4.3	Formation energy	31
4.4	Quantum effect: zero-point energy	34
5	Transition barriers between different charge states	37
5.1	Linearly interpolated reaction path	37
5.2	Reaction path with the extended nudged elastic band method	40

6	Hydrogen molecules in silica	43
6.1	Atomic configurations of molecular hydrogen complexes	43
6.2	Formation energy of molecular hydrogen complex	46
6.3	Vibrational frequencies of hydrogen molecules in silica	46
7	Conclusions	49

Chapter 1

Introduction

1.1 Hydrogen impurity in semiconductors

The hydrogen impurity is ubiquitous in all semiconductors[1]. Because hydrogen is highly diffusive and reactive, it can easily penetrate into samples and change their electronic and optical properties. There are two main motivations to study the effect of hydrogen impurity: intentional doping and unintentional contaminations. Intentional doping is performed in order to enhance properties of samples by passivating the existing dangling bonds. A typical example is amorphous silicon (*a*-Si), which is used in photovoltaics and thin film transistors. Before hydrogen doping, *a*-Si includes many dangling bonds, $10^{19}/\text{cm}^3$, which act as the electron-hole recombination centers and cause in-gap states. Because the dangling bonds degrade the performance, they should be removed. Hydrogen can passivate the dangling bonds and drastically reduce their numbers to 10^{15} - $10^{16}/\text{cm}^3$. The hydrogen doping is necessary to use *a*-Si in practice. Unintentional contamination of hydrogen sometimes causes an unexpected change of electronic properties. The example is ZnO, which is used in piezoelectric transducers and is a candidate for a blue and ultraviolet light emitter. ZnO always shows n-type conductivity. The origin of the conductivity had been a long-standing puzzle in spite of several decades of researches. Although intrinsic defects were first considered to be the origin because of the universality of the n-type conductivity, theoretical study showed that they could not explain the conductivity. First-principles calculations identified the cause, which is the hydrogen impurity. Although hydrogen is usually amphoteric impurity, which means hydrogen is a self-compensated impurity, it selectively behaves as a donor in ZnO. Unexpectedly, hydrogen impurity is the cause of the puzzling n-type conductivity. Hydrogen unintentionally penetrates into not only ZnO but also many other semiconductors because residual hydrogen contaminates samples in many growth techniques, such as chemical vapor deposition, sputtering, hydrothermal synthesis and molecular beam epitaxy. Therefore the effect of hydrogen impurity should be studied

in almost all the semiconductors.

Some of novel physics and technologies are driven by hydrogen. In iron-based superconductor, substitution of oxygen with hydrogen breaks the limit of electron doping, which is conventionally performed with the substitution with fluorine. The high electron doping reveals the hidden two-dome structure in phase diagram[2]. The superconductivity with the highest T_c is also achieved with a hydrogen-related material, hydrogen sulfide[3]. Hydrogen energy is a promising candidate for the next-generation energy system. Hydrogen energy system will be supported with technologies such as the photochemical splitting for hydrogen generation, hydrogen storage and hydrogen fuel cell.

Fundamental understanding of behaviors of hydrogen is important to facilitate the active use of hydrogen or suppress its detrimental behavior. In order to investigate and control the effect of hydrogen, both experimental and theoretical studies are indispensable.

Experimental detection of hydrogen impurity is rather difficult. Because hydrogen has no core electrons, x-ray photoluminescence cannot be used to detect the impurity. Secondary ion mass spectrometry (SIMS) is a powerful method to assess impurities quantitatively by destroying the surface of a sample and counting the secondary ions. Although SIMS is usually a high-sensitive method, its application to hydrogen is difficult because of the existence of hydrogens in residual gas. Nuclear reaction analysis (NRA) can detect hydrogen and even its depth profiling near a surface by using the nuclear reaction between ^{15}N and ^1H . Although NRA is promising to investigate the properties of hydrogen impurities, it is rarely applied to solids. Vibrational spectroscopies, infrared (IR) absorption and Raman scattering, can give the local vibrational modes (LVM) of defects. When hydrogen forms bonding to other atoms and a nonzero dipole moment exist, the LVM of the bonding can be detected by IR spectroscopy. Even if the dipole moment is zero, which is the case for hydrogen molecules in solids, Raman spectroscopy can measure the LVM when the polarizability changes by the vibration. The LVMs are useful to determine the charge and bonding state when combined with the first-principles estimation of vibrational frequencies. Electron spin resonance (ESR) and electron nuclear double resonance (ENDOR) can identify paramagnetic defects by the hyperfine coupling of electrons and a nucleus. These methods can be used to identify the isolate hydrogen impurity in solids. Muon spin rotation (μSR) experiment is an important method to study hydrogen impurity [4, 5, 6]. In μSR experiment, muon is used as a pseudo-isotope of hydrogen, which has 9 times smaller mass than hydrogen. μSR can give results similar to ESR experiments with high sensitivity. Although the μSR experiment is informative about hydrogen impurity, its result should be interpreted with taking into account the finite life time of muon, $2.2\mu\text{s}$, and its light mass. The finite life time may result the metastable state, not the thermodynamically stable state. The light mass yield large quantum effects and muon may not correspond to hydrogen. Electrical measurements, such as the deep level transient

spectroscopy (DLTS), may determine a position of defective in-gap state.

Theoretical study reveals many properties of hydrogen impurity [1, 7]. Because hydrogen impurity takes various atomic positions and electronic properties, which depend on its charge state and a host crystal, simple treatments such as the tight-binding method cannot be used. Therefore first-principles methods are necessary to study hydrogen impurities. Density functional theory (DFT) [8, 9] is the standard method to study defects in solids including hydrogen impurity because of its relatively low computational cost with including electron correlation. DFT can directly give microscopic properties of defects, such as charge density, LVMs and defect levels. These quantities can be compared with ESR (or μ SR) experiments, vibrational spectroscopies and DLTS, respectively. Furthermore, thermodynamical stability can be discussed with the formation energy, which is calculated with the total energies for various charge states of defects. The formation energy determines the population of defects. Because experimental quantitative analysis of hydrogen impurities are rather difficult, the calculated formation energy is important information.

1.2 Hydrogen impurity in silica: previous studies

Properties of hydrogen impurities in silica, SiO_2 , have been studied for its technological importance. Amorphous- SiO_2 ($a\text{-SiO}_2$) is especially important because of its application to wide variety of technologies, such as optical lenses, optical fibers and insulating layer of Si-based metal-oxide-semiconductor (MOS) devices. These applications are based on unique properties of $a\text{-SiO}_2$. The properties are its transparency from infrared to vacuum ultraviolet light, high chemical durability and high workability. Hydrogen sometimes improve the properties of SiO_2 -based technology. In MOS devices, many dangling bonds exist in the interface of Si and SiO_2 because of the lattice mismatch between them. Passivating the dangling bonds with hydrogen impurity is necessary for reliable operation of MOS devices. Another example is synthetic SiO_2 glass as an optical lens for photolithography. Ultraviolet light makes defects in SiO_2 , and the defects reduce the optical transparency. Doping hydrogen molecules improves the light durability of SiO_2 because hydrogen atoms released from the molecules can passivate dangling bonds induced by ultraviolet light. On the other hand, degradations are also caused by hydrogen impurity. In MOS devices, excess doping of hydrogen promotes dangling bonds at Si- SiO_2 interface because the excess hydrogen can depassivate the passivated dangling bonds by the formation of hydrogen molecules. In $a\text{-SiO}_2$, hydrogen breaks a weak elongated bond and generate a dangling bond. Hydrogen in silica is also studied from the perspectives of earth science because about 60 % of crust are made of silica.

To understand the behavior of hydrogen impurities, it is important to study two fundamental properties: thermodynamical stability and diffusion process.

As for thermodynamical stability, one of our prime concerns is the stability of isolated hydrogen (H^0) because there seems to be contradictions in ESR experiments and μ SR experiments. An experimental observation of isolated hydrogen atoms is especially difficult because the atoms do not show unique vibrational modes. Only the ESR or the μ SR experiments can be detect the H^0 atoms because they have an unpaired electron. In ESR experiments, H^0 atoms in silica are only detected with irradiated samples [10, 11, 12]. Without irradiation, no H^0 atoms are observed. The irradiation may generate the isolated hydrogen by breaking O-H or Si-H bonds. ESR experiments also show that the population of H^0 atom decreases exponentially when the temperature increases beyond around 100K. These facts indicate that the isolated hydrogen is not thermodynamically stable. On the other hand, μ SR experiments[13, 14] indicate the existence of a muonium (Mu^0), which is a pseudo isotope of a hydrogen atom composed of a positive muon and an electron. In μ SR experiments, majority of the incident muons is observed as Mu^0 . Furthermore, the population of $Mu^{+/-}$ becomes smaller when temperature becomes higher, and hence the population of Mu^0 seems to become larger by increasing the temperature. This indicates that the Mu^0 is thermodynamically stable and suggests that H^0 is also thermodynamically stable. This discrepancy between ESR experiments and μ SR experiments is usually assigned to the metastable feature of μ SR experiments due to finite lifetime of muon. However, the reason why Mu^0 is observed is not discussed furthermore.

Theoretical studies support the metastability of the H^0 state in silica. Thermodynamically stable charge states of hydrogen impurity have been investigated for various polymorphs of silica. The first theoretical study was performed by Yokozawa *et al.* for cristobalite[15]. They calculated the formation energy of three possible charge states of hydrogen impurity with local density approximation (LDA) within DFT and found that hydrogen impurity shows amphoteric behavior, which means that the charge state of the defect depends on the Fermi energy (or electron chemical potential). The isolated hydrogen atom (H^0) is not found to be thermodynamically stable. They also calculated LVMs of Si-H⁻ and O-H⁺ and concluded that these states can be detected by vibrational spectroscopies. Blöchl studied hydrogen impurity, and also hydrogen-related defects, in quartz SiO₂ with generalized-gradient approximation (GGA) of DFT[16]. Thermodynamically stable states are only H⁺ and H⁻ just like the case for cristobalite. Charge states of hydrogen impurity in amorphous SiO₂ is also studied by Godet *et al.*[17] with DFT-GGA. They prepared an amorphous structure and calculated the formation energies for several interstitial positions of H atom. Although the formation energy of H^0 is lower for larger interstitial voids, H^0 is not thermodynamically stable again, and H has an amphoteric feature. All these studies indicate that H^0 is not thermodynamically stable, and this is consistent with ESR experiments. However, the μ SR experiments cannot explained by these studies.

Diffusions of hydrogen atoms have been theoretically studied[18, 19]. Tuttle studied the diffusion of neutral atomic hydrogen in cristobalite with DFT-LDA and obtained the activation energy barriers about 0.2 eV, which is consistent with experimental values 0.05–0.2 eV[18]. Godet *et al.* studied the diffusion of H^+ (proton) in amorphous SiO_2 with DFT-GGA. The calculated activation energy, 0.50 eV, is in good agreement with experimental one, 0.38 eV[19]. Although these studies can explain experimental values related to diffusions, they assume that the charge state of hydrogen does not change during the diffusion. The hydrogen diffusion with changing its charge state is a concern of this study as described in the next section.

1.3 Purposes and outline of this study

Previous theoretical studies of hydrogen impurity in silica have two missing perspectives. The first one is the transitions between different charge states. In previous studies, only thermodynamically stable states were investigated, and the stability of metastable states was not discussed. Because the metastable states may be observed in μ SR experiments, the stability of metastable states should also be discussed. The charge state transition may also occur when hydrogen diffuses through samples. For example, hydrogen may change its charge state from H^+ via H^0 to H^- during a diffusion when the atom changes its position from a near-oxygen site via an interstitial site to oxygen vacancy. To treat such diffusion, the transition barrier between different charge states should be discussed.

The second one is the reliability of density functional theory to describe electronic structures of hydrogen impurities in silica. Previous theoretical studies are based on DFT, which has some shortcomings. The band-gap problem is a typical one, where conventional exchange correlation functionals, such as LDA or GGA, significantly underestimate the band gap. Hybrid functionals can improve the estimation of band gaps by partially taking the exact exchange term. However, their ability to describe the total energies is still under debate. Indeed, the hybrid Heyd-Scuseria-Ernzerhof functional, which is one of the most reliable functionals in solid-state calculations, sometimes predicts the wrong thermodynamically stable charge state[20].

Our purposes are to investigate these two missing points. For the first point, we studied the transition barriers between different charge states. The barriers were investigated with a linearly interpolated path between optimized structures and also with the optimized path. To calculate the optimized path, we extend the nudged elastic band method (NEB) [21], which is the standard method to calculate the minimum energy path between given two structures. In this study, the NEB method is extended to treat the minimum energy path over two different potential energy surfaces corresponding to two charge states. We discuss the stability of H^0 with the calculated transition barriers.

For the second point, we use the diffusion Monte Carlo (DMC) method [22, 23, 24] to simulate electronic structures from first principles. DMC is another method to treat defects in solids within reasonable computational time. In DMC, electronic structures are represented by a many-body wave function. DMC is in principle more accurate than DFT and actually is. DMC can describe wide variety of materials within small errors. It can estimate cohesive energies with errors within 0.1 eV compared to experimental values, lattice parameters with a several tenth of a percent and the band gaps within several tenth of eV. Furthermore, DMC can well describe strongly correlated materials[25, 26] or van der Waals systems[27], which are difficult to treat with DFT. DMC has also been applied to defective systems, such as self-interstitial in Si[28], vacancy in diamond[29] and Al[30], Schottky defect in MgO[31] and recently various defects in ZnO[20]. These studies show that DMC can well describe the experimental properties of defects. DMC has several shortcomings against DFT. A major one is that forces acting on ions are unfeasible in DMC because statistical sampling of the Hellman-Feynman force results in the divergence of statistical error and the force is indefinite. This means that atomic configurations cannot be relaxed with DMC. Another one is in evaluating physical quantities which do not commute with Hamiltonian. To evaluate the quantities, one must use the extrapolated estimators[22] which introduce some additional errors. We overcome these difficulties with complimentary use of DFT.

We studied the hydrogen impurity in two types of polymorphs of silica, quartz SiO_2 ($q\text{-SiO}_2$) and rutile SiO_2 ($r\text{-SiO}_2$, stishovite). Because silica is used for many technological applications as described in the previous section, the fundamental study of hydrogen in silica is very important. In μSR experiments of both systems, majority of muon is observed as muonium, and hence H^0 is suggested to be thermodynamically stable[14]. This is surprising because $r\text{-SiO}_2$ has 1.6 times larger density than $q\text{-SiO}_2$, and thus Mu^0 may be difficult to exist. Crystal structures of $q\text{-SiO}_2$ and $r\text{-SiO}_2$ are shown in Fig. 1.1. In $q\text{-SiO}_2$, a Si atom has a tetrahedral coordination. The tetrahedral coordination is common to many silica polymorphs, such as coesite or cristobalite, which differ from each other in the way to connect tetrahedra. On the other hand, a Si atom in $r\text{-SiO}_2$ has an octahedral coordination. Because of the difference of the coordination number, $q\text{-SiO}_2$ and $r\text{-SiO}_2$ have different electronic properties.

This thesis is organized as follows. Chapter 2 outlines first-principles methods to describe electronic structures and how to treat charge states of hydrogen impurities in this study. Chapter 3 describes the nudged elastic band method and its extension to calculate the transition barriers between different charge states. In chapter 4, the properties of an interstitial hydrogen atom in $q\text{-SiO}_2$ and $r\text{-SiO}_2$ is investigated with DMC. Chapter 5 shows the transition barriers between different charge states calculated with the method described in chapter 3. Chapter 6 illustrates possible forms of molecular complex of two

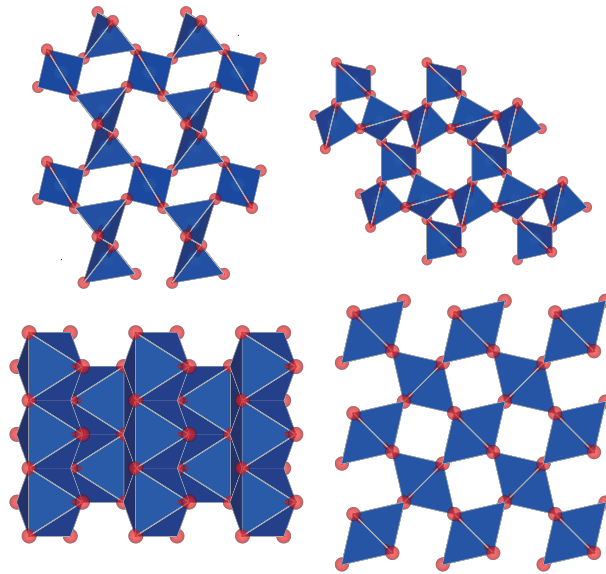


Figure 1.1: Crystal structures of quartz SiO₂ (upper) and rutile SiO₂ (lower). Left figures show the view from crystallographic a-axis and right figures from c-axis.

hydrogen impurities in *q*-SiO₂ and *r*-SiO₂ and its stability calculated with DFT and DMC. Chapter 7 presents conclusions and future perspectives of this study.

Chapter 2

Density functional theory and quantum Monte Carlo method

2.1 Density functional theory

Density functional theory (DFT) is the most standard method to simulate electronic systems of condensed matter from first principles. DFT is based on the celebrated Hohenberg-Kohn theorems [8]. The first theorem shows that the external potential of the electronic system can be determined only by the electron density of the ground state $n(\mathbf{r})$. Thus the ground state $|\Psi\rangle$ is a functional of $n(\mathbf{r})$. The second theorem states that the total energy $E[n]$ is variational in terms of $n(\mathbf{r})$,

$$E[n] = F[n] + \int v_{\text{ext}}(\mathbf{r})n(\mathbf{r})d^3r \geq E_0, \quad (2.1)$$

where $v_{\text{ext}}(\mathbf{r})$ is the external potential. $F[n]$ is the universal functional defined as

$$F[n] = \langle \Psi[n] | \hat{T} + V_{ee} | \Psi[n] \rangle, \quad (2.2)$$

which is independent of the external potential. The key quantity in DFT is this universal functional $F[n]$, which includes all the difficulty of the many-body problem. If this universal functional had been determined in a simple system such as electron gas, then any electronic system would be solved exactly.

The Kohn-Sham (KS) scheme [9] makes DFT-based simulation feasible. In the KS scheme, an interacting electron systems is mapped onto a fictitious noninteracting system, which has the same electron density as the interacting one. The scheme separates $F[n]$ into three parts,

$$F[n] = T_s[n] + E_h[n] + E_{xc}[n]. \quad (2.3)$$

The first part is the kinetic energy of the reference system. The second term is the Hartree term, which describes the classical Coulomb repulsion between electrons. The third term is

called the exchange-correlation functional, which is the rest part of $F[n]$. $E_{xc}[n]$ includes the remainder of the kinetic energy and the exchange-correlation interactions between electrons. This $E_{xc}[n]$ is the central quantity that determines how accurately interacting electrons is described. By this division, minimizing $E[n]$ results the KS equation,

$$\left[-\frac{1}{2}\nabla^2 + v_{\text{ext}}(\mathbf{r}) + v_h(\mathbf{r}) + v_{xc}(\mathbf{r}) \right] \psi_i(\mathbf{r}) = \epsilon_i \psi_i(\mathbf{r}), \quad (2.4)$$

$$v_{xc} = \frac{\delta E_{xc}[n]}{\delta n}, \quad n(\mathbf{r}) = \sum_i |\psi_i(\mathbf{r})|^2, \quad (2.5)$$

where the summation in Eq. (2.5) is taken for occupied orbitals. The ground state density and energy is obtained by solving this one-body self-consistent-field equation. By introducing the noninteracting reference system, the kinetic energy in $F[n]$ can be described accurately. Therefore, the KS scheme can reproduce the electron shells of atoms, which is essential to simulate condensed matter. This is a major advantage of the KS scheme compared to earlier density functionals such as the Thomas-Fermi method[32].

The conventional exchange correlation functional is the local density approximation (LDA) [33] and the generalized gradient approximation (GGA)[34]. They are parameterized by the accurate diffusion Monte Carlo simulation of homogeneous electron gas[35]. Because these functionals include part of electron correlation despite of its low computational cost, they have been used as the standard functional even in recent simulations. A major drawback of LDA and GGA is the underestimation of band gap of semiconductors and insulators, typically a half of the experimental one. This underestimation is due to an incomplete cancellation of self interactions in Hartree and exchange potentials (so-called self-interaction error or delocalization error)[36]. Hybrid functional overcomes this drawback to some extent by taking the Hartree-Fock exchange energy into the exchange functional. Especially, the Heyd-Scuseria-Ernzerhof (HSE) functional, which is a screened-hybrid functional, is one of the most succesful functionals to predict the band gap[37]. Although numerous exchange correlation functionals have been developed to improve accuracy, systematic improvements are difficult because the exchange correlation functional includes many-body physics.

These difficulties can be circumvented by another group of methods, wave function theories (WFTs). In WFTs, the many-body Hamiltonian are used without any modifications or simplifications. Therefore, although an approximated form of a trial wave function causes an error, the approximation can be actually improved systematically and the self-interaction does not exist in WFTs.

2.2 Quantum Monte Carlo method

Ab initio quantum Monte Carlo methods, the variational and diffusion Monte Carlo

method, can accurately describe correlated electrons in solids. We use the variational Monte Carlo method to optimize Slater-Jastrow trial wave functions. The optimized wave function is then used as the trial wave function in the diffusion Monte Carlo method.

2.2.1 Variational Monte Carlo method

In the variational Monte Carlo method (VMC) [23, 24], the many-body wave function is expressed as an explicitly correlated trial wave function $|\Psi_T\rangle$. The trial wave function is optimized with the variational principle and used to evaluate the physical quantity. The energy with the trial wave function, which is called the VMC energy E_{VMC} , is expressed as

$$E_{\text{VMC}} = \frac{\langle \Psi_T | \hat{H} | \Psi_T \rangle}{\langle \Psi_T | \Psi_T \rangle} = \int d^{3N} \mathbf{R} E_L(\mathbf{R}) \rho_{\text{VMC}}(\mathbf{R}). \quad (2.6)$$

Here $E_L(\mathbf{R})$ is the local energy defined as $E_L(\mathbf{R}) = \hat{H}\Psi_T(\mathbf{R})/\Psi_T(\mathbf{R})$, and $\rho_{\text{VMC}}(\mathbf{R}) = |\Psi_T(\mathbf{R})|^2/\langle \Psi_T | \Psi_T \rangle$. The integration are performed with the Monte Carlo method for computational efficiency.

The form of a trial wave function determines the electron correlation retrieved in VMC. In solid-state calculations, the trial wave function is almost always the Slater-Jastrow wave function, which is a product of a Slater determinant and a Jastrow factor. A Slater determinant is a mean-field wave function of a many-body system, where the orbitals are usually Hartree-Fock or Kohn-Sham ones. The Jastrow factor describes the explicit electron correlation, which is a function of the electron distances. In solid state calculation, the Jastrow factor usually has the electron-electron, the electron-ion and the electron-electron-ion terms[38]. The Jastrow factor is optimized with the Kato cusp condition[39]. The cusp condition is critical for efficient and stable simulations because the divergence of the local energy is removed by this condition.

Optimizing the trial wave function is critical in VMC. The optimization is also important in the diffusion Monte Carlo method because the statistical error largely depends on the quality of the trial wave function. The trial wave function is usually optimized with the variance minimization, which is based on the zero-variance principle. The zero-variance principle states that the variance of the energy would be zero if and only if the trial wave function were the exact eigenstate. Because the variance is positive when a trial state is not an eigenstate, the variance minimization is a reasonable way to optimize the wave function. To optimize variational parameters $\{\alpha\}$ in a trial wave function $\Psi_T^{\{\alpha\}}$, the variance is usually approximated as an unweighted variance,

$$\sigma_{\text{VMC}}^{2, \{\alpha\}, \{\alpha_0\}} = \int d\mathbf{R}^{3N} (E_L^{\{\alpha\}}(\mathbf{R}) - E_{\text{VMC}})^2 \rho_{\text{VMC}}^{\{\alpha_0\}}. \quad (2.7)$$

Here, $\{\alpha_0\}$ are the parameters used to generate the Monte Carlo distribution, and $\{\alpha\}$ are the variational parameters to be optimized. This optimization is repeated by updating

$\{\alpha_0\}$ until the variance is converged. The merits of this variance minimization is its stability and efficiency. Furthermore, high efficiency is achieved when only linear parameters are optimized[40].

A drawback of VMC is its strong dependence on the trial wave function. If total energies of different systems are compared to estimate, e.g., the cohesive energy or the formation energy, the choice of the trial wave function significantly affects the result because retrieved electron correlation is different from each other. This drawback can be suppressed with the diffusion Monte Carlo method discussed in the next section.

2.2.2 Diffusion Monte Carlo method

The diffusion Monte Carlo method (DMC) method is one of the most reliable methods to simulate the electronic structure of solids within reasonable computational time [23, 24]. DMC can retrieve the electron correlation missed with VMC by projecting out the lowest energy state in an initial trial wave function. This projection is realized by the imaginary-time Schrödinger equation. How the imaginary-time propagation works is easily understood by expanding an initial state by the eigenstates, $\Psi(\mathbf{R}, \tau = 0) = \sum_i c_i \Psi_i(\mathbf{R})$. The solution of the imaginary-time Schrödinger equation becomes $\Psi(\mathbf{R}, \tau) = \sum_i c_i \Psi_i(\mathbf{R}) \exp(-E_i \tau)$, where E_i is the energy of the eigenstate $\Psi_i(\mathbf{R})$. The propagation in imaginary time thus project out the most slowly decaying component, which is the ground state.

Although DMC is simple and elegant in principle, it suffers from the notorious fermion-sign problem to simulate electron systems. To circumvent the fermion-sign problem, the fixed-node approximation [41, 42] must be imposed. This approximation fixes the nodal surface of the ground state to that of a trial wave function, $\text{sign}[\Psi(\mathbf{R}, \tau)] = \text{sign}[\Psi_T(\mathbf{R})]$, in order to prevent the wave function from decaying to the ground state. The fixed-node approximation is imposed by the importance sampling. With the importance sampling, the wave function itself is not treated but the product of the wave function and the trial wave function, $f(\mathbf{R}, \tau) = \Psi(\mathbf{R}, \tau) \Psi_T(\mathbf{R})$ is. By assuming $f(\mathbf{R}, \tau) \geq 0$, the fixed-node approximation is imposed. The imaginary-time propagation of $f(\mathbf{R}, \tau)$ can be written as

$$-\frac{\partial}{\partial \tau} f(\mathbf{R}, \tau) = -\frac{1}{2} \nabla^2 f(\mathbf{R}, \tau) + \nabla \cdot [\mathbf{v}_D f(\mathbf{R}, \tau)] + [E_L(\mathbf{R}) - E_T] f(\mathbf{R}, \tau), \quad (2.8)$$

where $\mathbf{v}_D \equiv \Psi_T^{-1}(\mathbf{R}) \nabla \Psi_T(\mathbf{R})$ is the drift velocity, and $E_L(\mathbf{R})$ is the local energy. The most standard form of the trial wave function is the Slater-Jastrow wave function.

Although DMC can in principle treat electronic systems more accurately than other methods such as DFT, careful treatments of its approximations are necessary for reliable simulation. The sources of error are the fixed-node approximation, the pseudo-potential approximation, the finite-size error due to the inexact quantization of one-body orbitals

and the spurious periodic exchange-correlation hole and the finite-time-step error. We examined these errors and achieved the accuracy of 0.1 eV, as discussed later.

In this study, we use DMC for reliable estimations of the formation energy of hydrogen impurity. Besides DMC, perturbative methods such as the GW method are also known as accurate methods. They can accurately predict band gaps and the positions of in-gap states induced by impurity [43, 44, 45]. However, because the total energy is not feasible with the perturbative methods at present they cannot be used to estimate the formation energies of charged impurities, which is necessary to discuss the thermodynamical stability. Wave function theories (WFTs) commonly used in quantum chemistry are promising candidates to estimate total energy with high accuracy. Indeed, Møller-Plesset 2 (MP2) theory and the “gold standard” coupled-cluster (CC) theory have been used to calculate total energy of solid. These methods, especially CC with singles, doubles and perturbative triple excitations (CCSD(T)) method, accurately predict cohesive energies and band gaps of solids[46]. However, the computational costs of most WFTs are too high to treat the defective system. For example, the computational order is $O(N^5)$ for the MP2 method and $O(N^7)$ for the CCSD(T) method where N is the number of electron in the system. These high computational costs disable us to use such standard WFTs to simulate defective systems, which need simulations of large systems typically including several tenths to several hundreds of atoms.

2.3 Defective system

2.3.1 Charge state calculation

Defects may be charged up by exchanging electrons with other defects or impurities. Because it is time-consuming to treat multiple defects simultaneously, *ab initio* treatment of charged defects is performed with a charged system where only the target defect exists. In the charged system, the total charge of electrons does not match that of nuclei. Net charge in periodic systems produces the divergence of electrostatic interaction. The divergence is avoided by introducing uniform background charge which compensates for the net charge. Although the divergence can be avoided, spurious interactions arise due to the electrostatic interaction between the periodic defective charge and the background charge. This spurious interaction virtually reduces the energy of charged systems and should be corrected to compare the stability of various charge states. This effect of the spurious interaction is known as the finite-size effect because the effect depends largely on the size of the simulation cell and becomes zero when system size is infinite.

A traditional method to correct the finite-size effect is the Makov-Payne approximation[47], which is expressed as

$$E_{\text{corr}}^{\text{MP}} = E_{\text{PC}} + \frac{\beta}{\Omega} + \mathcal{O}(\Omega^{-5/3}). \quad (2.9)$$

Here, Ω is the volume of the simulation cell. The first term E_{PC} is the point-charge correction, which is the Madelung potential between the point charge on the defect position and the background charge. For anisotropic systems, E_{PC} is defined as $E_{\text{PC}} = -\frac{q}{2}V_{\text{PC}}$, and V_{PC} is [48],

$$V_{\text{PC}} = \sum_{\mathbf{R}_i} \frac{q}{\sqrt{|\bar{\epsilon}|}} \frac{\text{erfc}(\gamma\sqrt{\mathbf{R}_i \cdot \bar{\epsilon}^{-1} \cdot \mathbf{R}_i})}{\sqrt{\mathbf{R}_i \cdot \bar{\epsilon}^{-1} \cdot \mathbf{R}_i}} - \frac{\pi q}{\Omega\gamma^2} + \sum_{\mathbf{G}_i}^{i \neq 0} \frac{4\pi q}{\Omega} \frac{\exp(-\mathbf{G}_i \cdot \bar{\epsilon} \cdot \mathbf{G}_i/4\gamma^2)}{\mathbf{G}_i \cdot \bar{\epsilon} \cdot \mathbf{G}_i} - \frac{2\gamma q}{\sqrt{\pi|\bar{\epsilon}|}}, \quad (2.10)$$

where \mathbf{R}_i and \mathbf{G}_i are real and reciprocal lattice vectors, respectively. $\bar{\epsilon}$ is the dielectric tensor and γ is a convergence parameter. The second term in Eq. (2.9) retrieves the interaction arising from higher order terms of defective charge such as a dipole moment. This term can be calculated with either estimating defective charge or extrapolating energies into the infinite system size. In this study, we performed the extrapolation as shown in Fig. 4.1.

2.3.2 Formation energy

The most stable charge state can be determined by the formation energy, which is the difference of energies between the defective system and the reference system (Fig. 2.1). The number of electrons and the impurity atom are different between these systems, and the differences are compensated with the chemical potentials of electrons and impurities, respectively. The electron chemical potential is conventionally notes as the Fermi energy. Because the Fermi energy is determined by the other defects present in a sample, the Fermi energy depends on the way to prepare the sample.

The formation energy of hydrogen impurity is formulated as

$$E_f[H^q] = (E_{\text{tot}}[H^q] - E_{\text{tot}}[\text{perfect}]) - n_H\mu_H + q(\mu_{\text{VBM}} + E_F) + E_{\text{corr}}[H^q], \quad (2.11)$$

where H^q means the hydrogen impurity with charge state q . $E_{\text{tot}}[H^q]$ and $E_{\text{tot}}[\text{perfect}]$ is the total energy of a defective system and pristine system, respectively. n_H is the number of impurity hydrogen and μ_H is its chemical potential. μ_{VBM} is the energy of the valence band maximum (VBM) and E_F is the Fermi energy relative to VBM. $E_{\text{corr}}[H^q]$ represents the finite-size correction discussed in the previous section. The most stable charge state is the state that has the lowest formation energy.

Typical formation energies are shown in Fig. 2.2. Because the formation energy depends on the Fermi energy, Thermodynamically stable state also depends on the Fermi energy. The stability of the neutral defect can be discussed with the U_{eff} parameter[49] defined as

$$U_{\text{eff}} = E_f^{q+1} + E_f^{q-1} - 2E_f^q. \quad (2.12)$$

U_{eff} can be sketched graphically as in Fig. 2.2. U_{eff} is the effective Coulomb interaction between electrons on the same defective site. Different from the Hubbard U parameter,

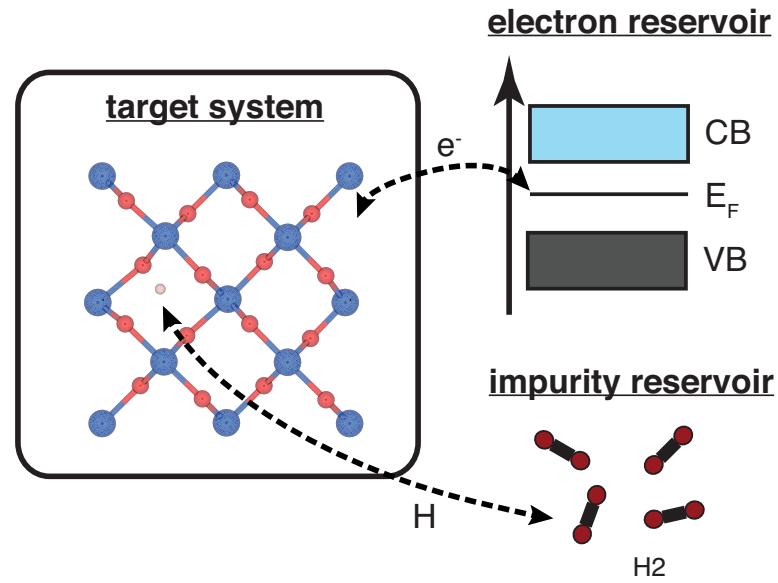


Figure 2.1: A schematic illustration of the formation energy.

U_{eff} includes not only the electrostatic interaction but also the effect of lattice relaxation. If the lattice relaxation largely affects the stability, U_{eff} may become negative. Negative U_{eff} means that the state of charge q is not stable thermodynamically and favors to form the $q + 1$ and $q - 1$ impurities, e.g. $2\text{H}^0 \rightarrow \text{H}^+ + \text{H}^-$. Another important quantity is the thermodynamic transition level $\epsilon(+/-)$, which is defined as the Fermi energy where positive and negative charge states have the same formation energy. If the Fermi level is below $\epsilon(+/-)$, positive charge state is thermodynamically stable, and vice versa.

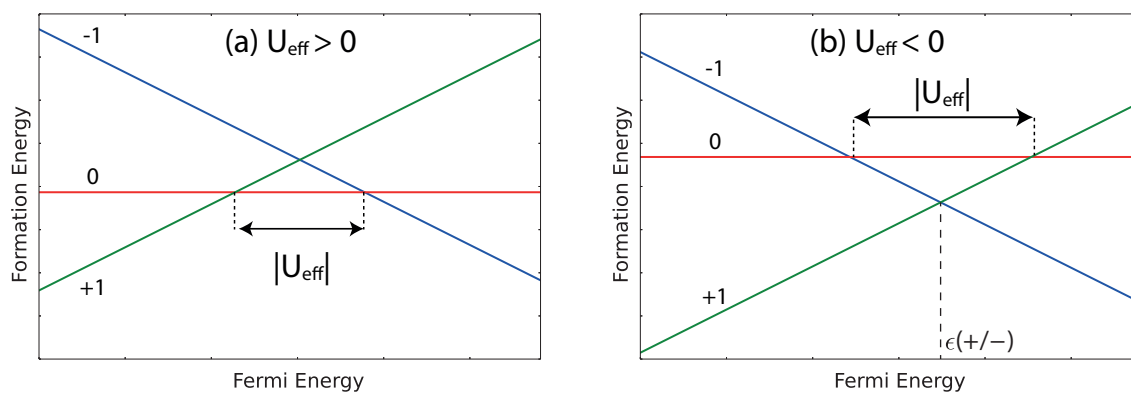


Figure 2.2: A typical formation energy for (a) $U_{\text{eff}} > 0$ and (b) $U_{\text{eff}} < 0$. The definition of the thermodynamic transition level $\epsilon(+/-)$ is also shown.

Chapter 3

Nudged elastic band method for transition barriers between different charge states

3.1 Nudged elastic band method

The nudged elastic band (NEB) method is a method to find the minimum energy path (MEP) between a given initial and final state[21, 50]. The NEB has been used to analyze chemical reactions[51], diffusion of interstitial impurities in solids[52, 53], and so on. The reaction rate between the two states is determined by the activation energy, which is the highest energy on the MEP.

In the NEB method, a string of images (replicas) of the systems are used to describe the MEP (Fig. 3.1). Each image has a different atomic configuration. Initial images are usually prepared by the linear interpolation between the initial and final state. Then the images are relaxed to locate on the MEP. The forces acting on the images are made of two kind of forces, the true force perpendicular to the path and the spring force parallel to the path. The former is the force by the potential energy surface and ensure that the images locate on the MEP. The latter is a spurious force that makes the distances between adjacent images equal. Images relaxed with this forces are equally arranged on the MEP and thus express the MEP.

The detailed formulation of the forces in the NEB method is as follows,

$$F_i^{\text{NEB}} = F_i^{\text{true}\perp} + F_i^{\text{spring}\parallel}, \quad (3.1)$$

$$F_i^{\text{true}\perp} = F_i^{\text{true}} - (F_i^{\text{true}} \cdot \tau_i)\tau_i, \quad (3.2)$$

$$F_i^{\text{spring}\parallel} = k(|R_{i+1} - R_i| - |R_i - R_{i-1}|)\tau_i, \quad (3.3)$$

where F_i^{NEB} is the NEB force acting on the image i . τ_i is the unit vector along the path on

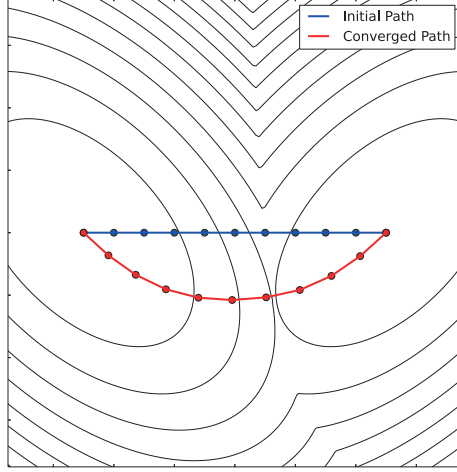


Figure 3.1: A schematic illustration of the NEB method.

the image i . τ_i changes its direction when the path changes. $F_i^{\text{true}\perp}$ is the perpendicular component of the force by the potential energy surface, which is the Hellman-Feynman force in this study. $F_i^{\text{spring}\parallel}$ is the parallel component of the spring force by adjacent images. k is the spring constant, which does not affect the converged path. The spring force is evaluated with the distance between adjacent images in order to ensure the equal intervals between images.

For stable calculations, $\{\tau_i\}$ are expressed by the improved tangent[21]. Its formulation is

$$\tau_i = \begin{cases} \tau_i^+ & E_{i+1} > E_i > E_{i-1}, \\ \tau_i^- & E_{i+1} < E_i < E_{i-1}, \end{cases} \quad (3.4)$$

where

$$\tau_i^+ = R_{i+1} - R_i, \quad \tau_i^- = R_i - R_{i-1}. \quad (3.5)$$

Here, E_i is the energy of image. If the energies of both adjacent images are lower or higher than an image i , which means $E_{i+1} < E_i > E_{i-1}$ or $E_{i+1} > E_i < E_{i-1}$, τ_i is calculated by weighted average of τ_i^+ and τ_i^- ,

$$\tau_i = \begin{cases} \tau_i^+ \Delta E_i^{\text{max}} + \tau_i^- \Delta E_i^{\text{min}} & E_{i+1} > E_{i-1} \\ \tau_i^+ \Delta E_i^{\text{min}} + \tau_i^- \Delta E_i^{\text{max}} & E_{i+1} < E_{i-1} \end{cases} \quad (3.6)$$

where

$$\Delta E_i^{\text{max}} = \max(|E_{i+1} - E_i|, |E_{i-1} - E_i|) \quad \Delta E_i^{\text{min}} = \min(|E_{i+1} - E_i|, |E_{i-1} - E_i|). \quad (3.7)$$

The images are relaxed until the residual forces, $|F_i^{\text{NEB}}|$, is less than a tolerance, F_{tor} .

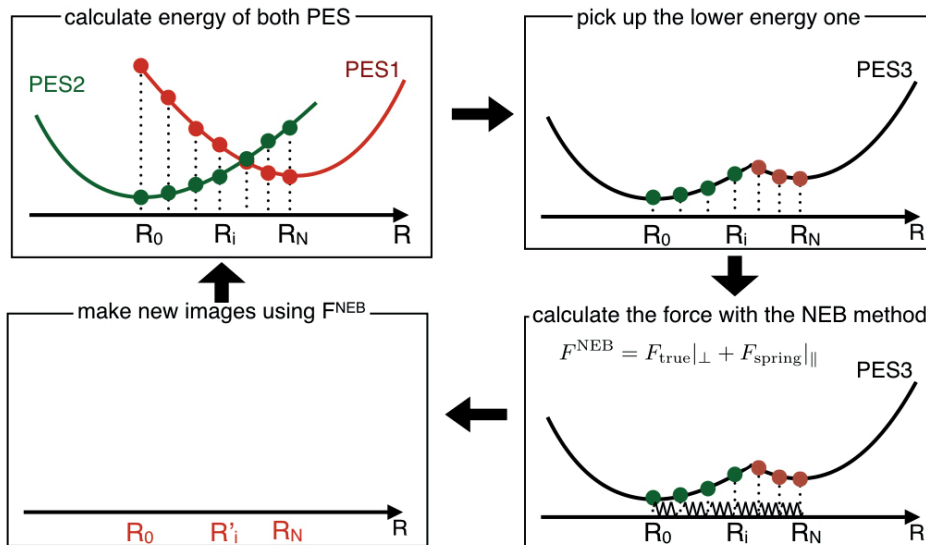


Figure 3.2: A schematic illustration of the extended NEB method.

The computational efficiency of the NEB method depends on the choice of the optimization method [54]. In this study, we used the conjugate-gradient (CG) method to optimize the configurations of images. Although the CG method is not the most efficient for the NEB method, we choose the method because its implementation is easy.

3.2 Extended nudged elastic band method

Although the NEB method is a powerful method to calculate the MEP, the method cannot be used to obtain the transition barrier between different charge states because each charge state has a different PES. In order to treat the MEPs over different charge states, we extended the NEB method.

Figure 3.2 illustrates the extended NEB method. In this method, we always calculate the total energies of both PESs with an atomic configurations of each images. Then we choose the lower energy one at each image to construct another PES, labeled PES3. The NEB forces are evaluated for PES3, and the images are updated with the forces. For updated images, we calculate the total energy of both PESs again, and repeat the procedure. This procedure is repeated until the NEB forces are less than some tolerance, as the same way in the standard NEB method.

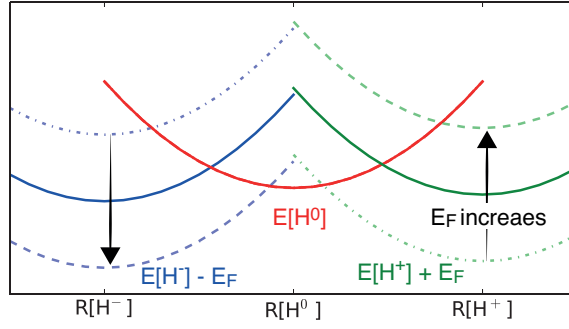


Figure 3.3: A schematic picture of the potential energy surface (PES) calculated in this study. The dependence of PESs on the Fermi energy E_F is illustrated. In some Fermi energy, finite transition barriers exist.

In our calculation, two PESs correspond to the different charge states of hydrogen impurity in silica. Because different charge states have different numbers of electrons, the total energies should be corrected to compensate the difference. In the same way as the formation energy, we correct the total energy with the electron chemical potential, or the Fermi energy. Thus the corrected energies of the negative, neutral and positive states is $E_{\text{tot}}[\text{H}^-] - qE_F$, $E_{\text{tot}}[\text{H}^0]$ and $E_{\text{tot}}[\text{H}^+] + E_F$, respectively. Therefore, transition barriers depend on the Fermi energy (Fig. 3.3). The lower the Fermi energy is, the more stable the H^+ state is and the more unstable H^- state is. Because the MEP depends on the Fermi energy, the accurate estimate of the transition barrier requires to evaluate the MEP at each Fermi energy.

We developed a code of this NEB method and combined it to xTAPP code, which is a first-principles plane-wave pseudopotential code. We used the method to study the stability of metastable charge states of hydrogen impurity in silica.

Chapter 4

Isolated hydrogen atom in silica

In this chapter, we discuss the stability of an isolated hydrogen in quartz SiO_2 and rutile SiO_2 (abbreviated as $q\text{-SiO}_2$ and $r\text{-SiO}_2$ hereafter) using the reliable diffusion Monte Carlo method. Firstly, the relaxed atomic configurations and the density of states of hydrogen impurity are shown for three possible charge states, H^- , H^0 and H^+ . Then the most stable charge state is investigated with the formation energy. To compare the results with μSR experiments, the quantum effect of muon is considered within the zero-point energy.

4.1 Computational details

4.1.1 Density functional theory

We used the eXtended Tokyo Ab-initio Program Package (XTAPP) code [55, 56] for DFT calculations with the Perdew-Burke-Ernzerhof (PBE) exchange-correlation functional[34], which is based on the generalized-gradient-approximation (GGA). The norm-conserving pseudopotentials were used with a plane-wave basis set with an energy cutoff of 100 Ry. We optimized the lattice parameters for the pristine crystals with the gamma-centered k-point meshes of $6 \times 6 \times 6$ both for $q\text{-SiO}_2$ and $r\text{-SiO}_2$ until residual stress were below 0.05 GPa. While optimizing the lattice structures, we kept the cutoff energy constant with the method of Bernasconi *et al.*[57]. The optimized lattice structures were also used to calculate the defective systems. The atomic configurations of defective systems were optimized with $2 \times 2 \times 2$ k-point meshes until residual forces were below 0.01 eV/Å. The total energies of charge states were corrected by the Makov-Payne method[47] (see section 2.3.1) with the extrapolation using supercells containing 73, 109 and 163 atoms. The extrapolation for $r\text{-SiO}_2$ is illustrated in Fig. 4.1. Whereas larger supercells do not change the calculated formation energy of the H^0 state, the other charge states are largely affected and should be extrapolated to the infinite size of the supercell.

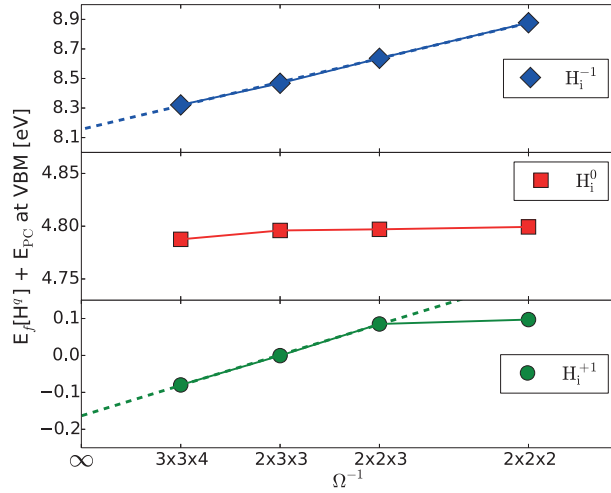


Figure 4.1: The Makov-Payne corrections of the formation energies of hydrogen impurity in r -SiO₂ calculated with the GGA-PBE functional. The linear extrapolation was performed using from $2 \times 2 \times 3$ to $3 \times 3 \times 4$ super cells.

4.1.2 Diffusion Monte Carlo method

Quantum Monte Carlo (QMC) calculations were performed with the CASINO code[23]. The trial wave function is the Slater-Jastrow wave function where the Slater determinant consists of the Kohn-Sham orbitals calculated with the GGA functional. The orbitals are firstly prepared in the plane-wave basis with the xTAPP code[55, 56] and then converted into the blip-function basis[58], which is a very efficient localized basis. We used the natural spacing of the blip grid as $a = \pi/k_{\max}$, where k_{\max} is the cutoff of the wave vector. The convergence of one-body orbitals were checked by increasing the plane-wave cutoff energy and comparing DMC energies. We found that the stable DMC simulation requires the plane-wave cutoff of 144 Ry for q -SiO₂ and 121Ry for r -SiO₂. These relatively large cutoff energies are necessary for stable calculations of the transition barriers between the charge states, discussed later.

We checked the fixed-node error by comparing the formation energies calculated with DMC using the GGA, the Hartree-Fock[59] and the hybrid PBE0[60] orbitals. All these fixed-node DMC calculations show almost the same formation energies. Their differences are within 0.1eV, which is the typical statistical error in this study. Therefore, we conclude that the choice of one-particle orbitals does not affect our results. The nodal surface may be improved by many-body wave functions beyond the Slater-Jastrow wave function, such as the backflow wave functions[61] or pairing wave functions[62]. However, such a wave function is very time-consuming to use in solid state calculations and is therefore beyond the scope of this study.

Table 4.1: The ionization potentials of SiH₄ and H₂O molecule (in eV). Statistical errors of DMC calculations are shown in parenthesis. ^a Reference[65]. ^b Reference[66].

	GGA	DMC	Exp.
SiH ₄	11.95	12.68(3)	12.6 ^a
H ₂ O	12.51	12.68(3)	12.61 ^b

The Jastrow factors included the electron-electron (e-e), electron-ion (e-i) and electron-electron-ion (e-e-i) terms. We used the standard formulation of the Jastrow factor used in solid state calculations[38]. The Jastrow factors were optimized by minimizing the unreweighted variance, which is known to be very stable and efficient[40]. We used the same Jastrow factors for the same atomic species in each charge system. This means that if, for example, a Si atom forms chemical bonding with hydrogen impurity, we use the same Jastrow factor for the Si atom as that for other Si atoms. This treatment may give inaccurate Jastrow factors, and they may cause instability or sizable errors in the DMC simulation. To verify our Jastrow factors, we calculated the DMC energies of smaller systems with Jastrow factors where H-bonded atoms have different parameters from other atoms. We confirm that our Jastrow factor has sufficient accuracy by comparing the DMC energies with the Jastrow factor and our Jastrow factor.

In QMC calculations, we used the same norm-conserving pseudopotentials as the GGA calculations. Because the pseudopotential is not made for QMC calculations, this may be another source of error. Our pseudopotentials are verified by calculating the ionization potential (IP) of SiH₄ and H₂O molecules. Table. 4.1 shows the calculated IPs. Because the experimental IPs are well reproduced by DMC calculations, the pseudopotentials seem to give no additional error for DMC calculations. The non-local part of the pseudopotentials were treated by the localization approximations[63]. We also used the Casulas' t-move scheme[64] to estimate the error caused by the localization approximation, and got the difference of the formation energies within 0.1 eV.

Other sizable errors may be caused by the imaginary time step and the finite number of a twist grid in the twisted-boundary condition[67]. We checked the convergence of the DMC energies about these conditions by decreasing the time step and increasing the number of the grids. To achieve the error within 0.1 eV, we used the time step of 0.02 a.u. and the grids of $2 \times 2 \times 2$ for both *q*-SiO₂ and *r*-SiO₂.

The valence band maximum (VBM) and the conduction band minimum (CBM) were estimated with the formula $E[N] - E[N - 1]$ and $E[N + 1] - E[N]$, respectively. Each value is extrapolated to the infinite system size in order to remove the finite-size effect.

All the DMC calculations were performed using the supercomputers at the Institute for Solid State Physics, the University of Tokyo. We typically used 144 nodes (12cores/nodes) and kept the number of walkers for DMC 10 walkers/core. We performed statistical sampling of 4800 imaginary-time steps after initial 200 steps for projecting out the ground state and achieved the statistical error of 0.0025eV/SiO₂ (or 0.06 eV per simulation cell, which consists of Si₂₄O₄₈H)

4.2 Relaxed structures and density of states

Hydrogen impurity may take three possible charge states, H⁺, H⁰ and H⁻. We optimized the atomic configurations of each charge states using DFT with the PBE functional[34]. Figure 4.2 shows the optimized structures of *q*-SiO₂ and *r*-SiO₂. The optimum position of H atom largely depends on its charge state. H⁺ forms a chemical bonding with an O atom while H⁻ with a Si atom. These chemical bondings are reasonable because O atoms and Si atoms are negatively and positively charged, respectively. H⁰ is located at the interstitial void of SiO₂ with no chemical bond. This state is the isolated hydrogen, which can be observed experimentally in ESR and μ SR experiments due to its finite spin density.

The optimized atomic configurations of *q*-SiO₂ are consistent with a previous study[17]. In H⁻ state, the Si atom moves to the surface of the oxygen tetrahedra, and a bipyramidal structure is formed. H⁰ is at the position with the maximum distance, 2.37Å, from oxygen atoms. The bond lengths are 1.02Å for O-H in H⁺ and 1.50Å for Si-H in H⁻. In *r*-SiO₂, the hydrogen impurity is on the ab-plane where Si atoms and O atoms exist. The bond lengths of Si-H and O-H are 1.38Å and 1.01Å, respectively. The distance between H⁰ and the nearest oxygen atoms are 1.73Å, which is shorter than that of *q*-SiO₂ because of smaller interstitial voids.

The density of states (DOS) of *r*-SiO₂ and *q*-SiO₂ are shown in Fig. 4.3. The electronic structure of silica is assigned to the major contributions of ionic bondings and the minor contributions of covalence bondings. The valence band mainly consists of 2*s* and 2*p* orbitals of oxygen atoms because of the high ionicity. The small covalency add the components of 3*s* and 3*p* orbitals of silicon atoms to the valence band. The conduction bands are well described by the orbitals of Si atoms. In the H⁰ state, there is an in-gap state which has the feature of 1*s* orbital of hydrogen. Except for the in-gap state, the entire DOS is similar to that of the pristine crystal. This indicates that the hydrogen is isolated without any chemical bonding as expected from the atomic configuration. In the H⁺ state, hydrogen state locates below the O 2*s* states due to hybridization of H 1*s* and O 2*s* orbitals in O-H bonding.

The structural optimization using DMC was also performed in order to study its effect on the stability of the H⁰ state. Because the ionic forces were not feasible in usual DMC

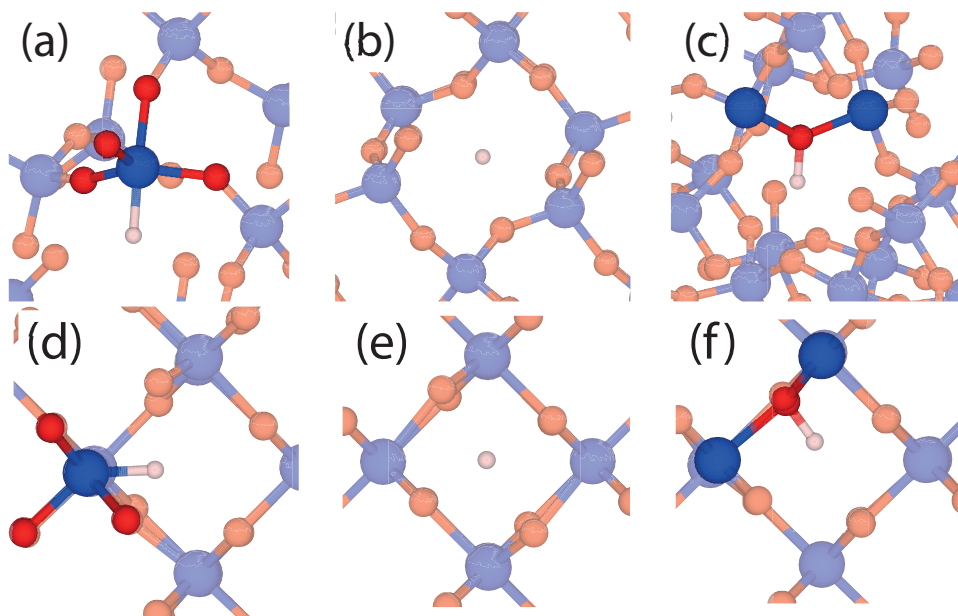


Figure 4.2: Optimized atomic configurations of (a) H^- , (b) H^0 and (c) H^+ for q - SiO_2 and (d) H^- , (e) H^0 and (f) H^+ for r - SiO_2 .

simulations[68], we prepared candidates of optimized structures and compared their energies. The candidates were constructed with the linear interpolation and extrapolation between the pristine and H^0 structures optimized with the GGA calculations. The extrapolation was considered up to the 150 % lattice distortion of the H^0 state. The resulting energy variation for r - SiO_2 is shown in Fig. 4.4. Figure 4.4 illustrates that the effect of the structural optimization is at most 0.1 eV. Because the interstitial voids are smaller in r - SiO_2 than in q - SiO_2 , the effect of optimizing structure may be smaller in q - SiO_2 . Therefore we conclude that the stability of H^0 is not affected by the structural optimization with DMC both in r - SiO_2 and in q - SiO_2 . Although the relaxation with DMC does not affect the H^0 state, other states may be affected by, e.g., optimizing the bond length. However, because our main concern was whether isolated hydrogen atom exists or not, we did not perform the structural optimization of other charge states.

4.3 Formation energy

We investigated which charge state of hydrogen impurity is the most stable in silica in terms of the formation energy. The formation energy was calculated with DFT and DMC.

The formation energy calculated with GGA is shown in dotted line in Fig. 4.5. The range of the Fermi energy is between VBM and CBM calculated with GGA. The origin of the Fermi energy is taken as VBM calculated with DMC. The calculated thermodynamic

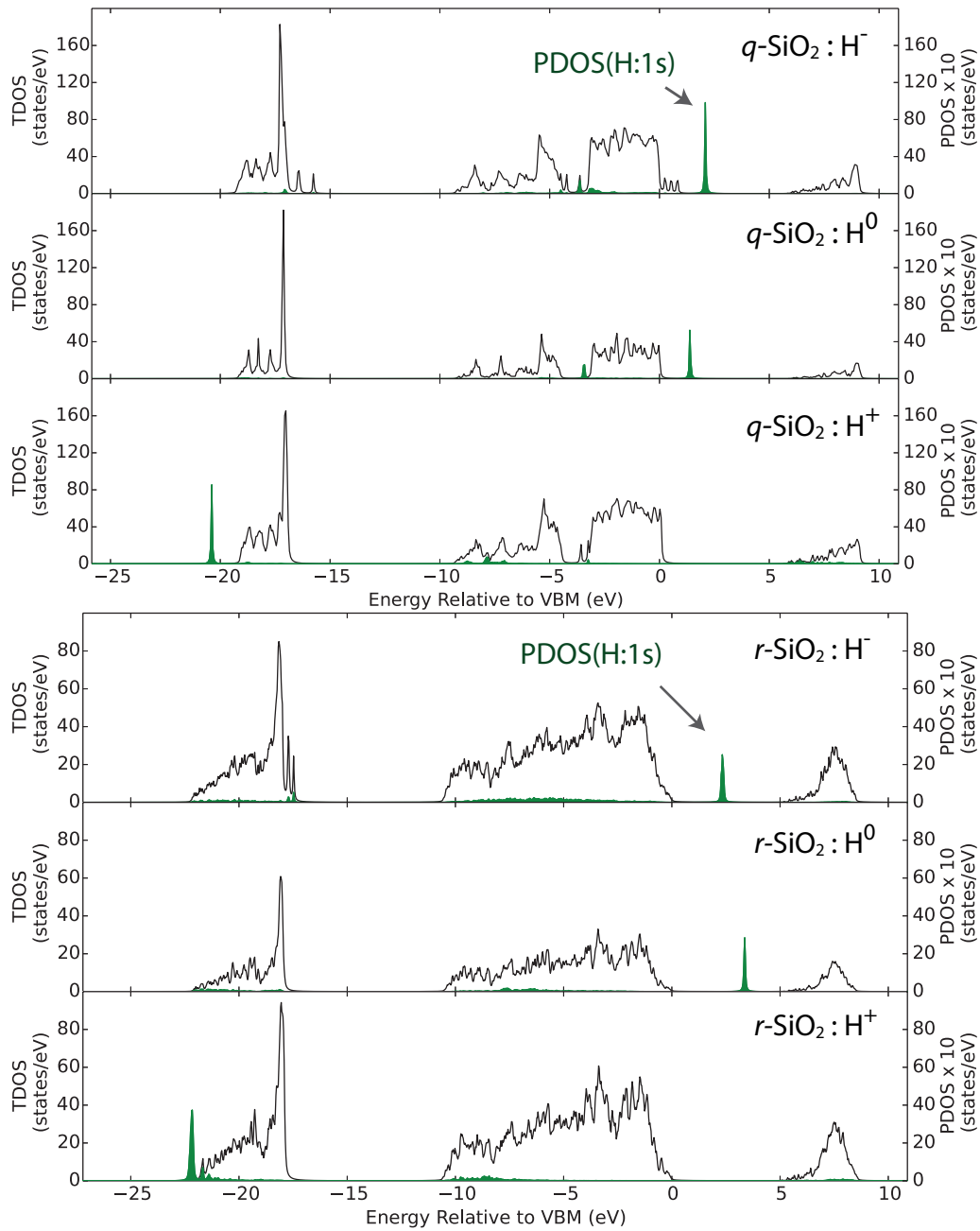


Figure 4.3: Density of states for hydrogen impurities of each charge states calculated with $\text{Si}_{24}\text{O}_{48}\text{H}$ structure using the GGA functional. The upper panel corresponds to $q\text{-SiO}_2$ and the lower panel to $r\text{-SiO}_2$. In each panel, the density of states of H^- , H^0 and H^+ are shown in the upper, middle and lower figure, respectively.

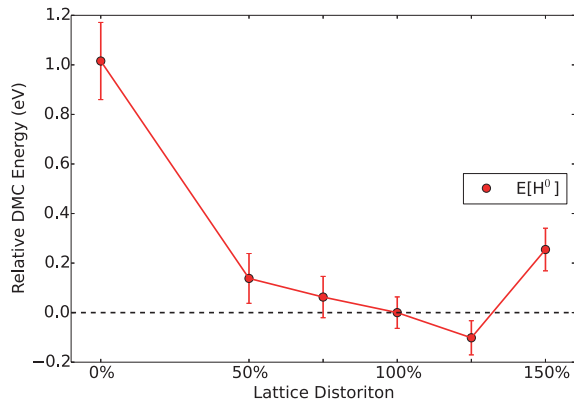


Figure 4.4: Structural optimization of the H^0 state in r - SiO_2 using DMC. The structure of host crystal is that of the pristine crystal for 0%, that of the GGA optimized structure for 100% and the over-relaxed structure for 150%.

transition levels $\epsilon(+/-)$ with GGA calculation are 3.8 eV in q - SiO_2 and 4.8 eV in r - SiO_2 . The U_{eff} parameter is -0.4 eV and -1.7 eV in q - SiO_2 and r - SiO_2 , respectively. The formation energy of q - SiO_2 is consistent with the previous study[17]. The negative U_{eff} behavior appears in both systems, and the isolated hydrogen, H^0 , is predicted to be unstable in these systems.

The formation energy was also evaluated with DMC (solid line in Fig. 4.5). The formation energy is plotted in the region between VBM and CBM calculated with DMC. DMC changes the formation energy calculated with GGA in a different fashion for q - SiO_2 and r - SiO_2 . For q - SiO_2 , little variations of $E_f[H^-]$ and $E_f[H^0]$ were observed whereas $E_f[H^+]$ decreased about 0.6 eV. On the other hand, for r - SiO_2 , $E_f[H^-]$ increases about 1.8 eV and $E_f[H^0]$ and $E_f[H^+]$ shows little change. This difference may be due to the different bonding characters between q - SiO_2 and r - SiO_2 . In q - SiO_2 , the coordination number of Si and O atom is 4 and 2, respectively, while the coordination number is 6 and 3 in r - SiO_2 . Because the electron correlation in these systems are different from each other, the explicitly correlated DMC method give qualitatively different predictions from GGA.

The thermodynamic transition level and U_{eff} is 6.4 eV above VBM and -1.1 eV for q - SiO_2 and 6.9 eV above VBM and -0.4 eV in r - SiO_2 . The different effects of DMC causes the large opposite correction for U_{eff} . The values of U_{eff} are still negative for both systems. Therefore, we conclude that the H^0 state is metastable for all the range of the Fermi energy in these systems. This result supports the prediction of ESR experiments[11, 12] and is opposite to that of μSR experiments[13, 14] (see section 1.2).

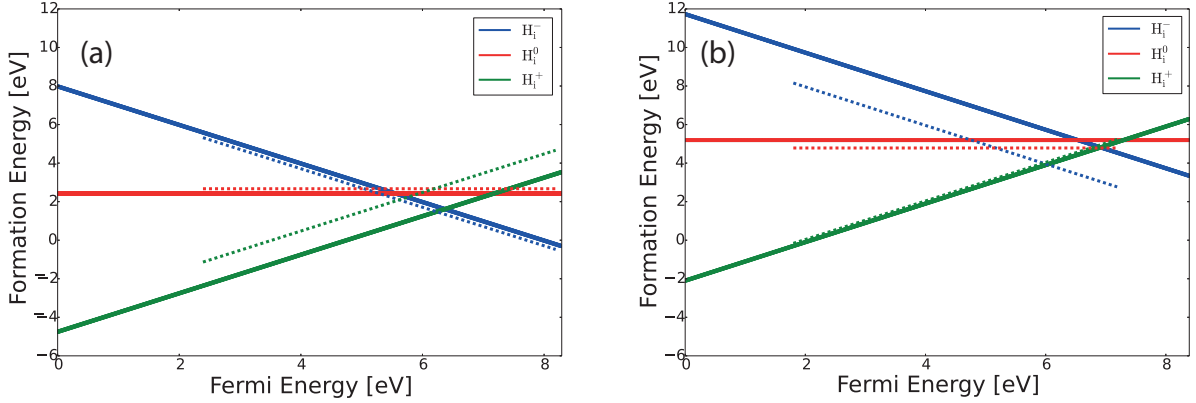


Figure 4.5: The formation energy of three charge states of hydrogen impurity in (a) q -SiO₂ and (b) r -SiO₂. Solid lines represent the formation energy calculated with DMC and dotted lines with GGA.

4.4 Quantum effect: zero-point energy

The results in the previous section cannot explain the μ SR experiments where the majority of incident muons are observed as muonium, which is a counterpart of H^0 made of a positive muon (μ^+) and an electron. The main difference between a positive muon and a proton is their mass. Because muon has 9 times smaller mass than proton, the quantum effect may largely affect the stability of Mu. In order to discuss the stability of Mu⁰, we corrected the formation energies with the zero-point energy (ZPE). Because each charge state has different bonding character, ZPE is also different from each other. Because Mu⁰ locates at the interstitial void of the host crystal without any bonding, its ZPE is lower than other charge states.

In order to estimate the ZPEs, we evaluated the dynamical matrix with the frozen-phonon method using GGA-PBE calculations. The calculation was performed with the defective systems, which contain not only the host SiO₂ but also the hydrogen impurity. The vibrational frequencies were estimated by diagonalizing the dynamical matrixes. Because evaluating the vibrational frequencies with DMC is rather challenging due to its high computational cost and statistical error, we use GGA-PBE to calculate the frequencies. In molecular systems, the error in calculated vibrational frequency with PBE is typically 100 cm⁻¹[69], which is about 0.01 eV. Therefore, PBE seems to be accurate enough to estimate vibrational frequencies in our purpose. The light mass of muon produces three localized phonon modes. Using the frequencies of these modes, $\{\omega_i\}_{i=1}^3$, ZPE was evaluated as $ZPE = \sum_i \frac{1}{2} \hbar \omega_i$.

Table 4.2 shows the calculated ZPEs for q -SiO₂ and r -SiO₂. Common to both systems,

Table 4.2: The zero-point energies of Mu and H in each charge state (in eV).

	<i>q</i> -SiO ₂			<i>r</i> -SiO ₂		
	+	0	-	+	0	-
Mu	0.93	0.33	0.75	1.03	0.58	0.96
H	0.31	0.11	0.25	0.34	0.19	0.32

the Mu^+ and Mu^- states have larger ZPEs than the Mu^0 state. This is because the $\text{Mu}^{+/-}$ state forms chemical bonding to other atoms whereas no chemical bonding exists for the Mu^0 state, as mentioned before. The difference in ZPE between Mu^0 and other states increases U_{eff} and thus increases the relative stability of Mu^0 compared to other charge states. The ZPE of Mu^0 is lower in *q*-SiO₂ than in *r*-SiO₂. This may be due to the larger size of interstitial voids in *q*-SiO₂. Adding the ZPEs to the formation energies calculated with DMC, the value of U_{eff} increases from -1.1 eV to -0.6 eV in *q*-SiO₂ and from -0.4 eV to 0.0 eV in *r*-SiO₂. Mu^0 may thus be the most stable in *r*-SiO₂ at some Fermi energies. However, the region of the Fermi energy where Mu^0 is the most stable is very narrow. Therefore, this result cannot explain μSR experiments that indicate that Mu^0 is the most stable state.

Other quantum effects, such as the quantum tunneling, may affect the stability of Mu^0 . Although these effects may be important to discuss $\text{Mu}[70]$, the effects are beyond the scope of this study.

Chapter 5

Transition barriers between different charge states

The formation energies presented in the previous chapter indicate that the isolated hydrogen (H^0) is not the most stable in silica. To study the stability of the metastable H^0 state, we calculated the transition barriers between different charge states.

5.1 Linearly interpolated reaction path

Firstly, we took the reaction path as the linear interpolation between the optimized structures of each charge states. For example, the linear path between the H^0 state and the H^+ state is $R_\alpha[\text{H}^0 \rightarrow \text{H}^+] = \alpha R[\text{H}^0] + (1 - \alpha)R[\text{H}^+]$, where $R[\text{H}^0]$ and $R[\text{H}^+]$ are the optimized atomic positions of all atoms and α is a parameter of the interpolation taking the values in $0 < \alpha < 1$.

The potential energy surfaces (PESs) of q - SiO_2 and r - SiO_2 are shown in Fig. 5.1. The calculated PESs depend on the Fermi energy of the system as discussed in section 3.2. The Fermi energy is taken as the thermodynamic transition level $\epsilon_{\text{DFT}}(+/-)$ or $\epsilon_{\text{DMC}}(+/-)$, corresponding to the computational method. DMC calculations were performed only for the circular points. The intervals were interpolated using the DFT results. The interpolation was performed with adding a linear function to the DFT curves to match the corrected DFT energies and the calculated DMC energies. By comparing DMC and DFT, DMC generally increases the calculated energies of each charge states with inconsistent atomic configurations, such as the H^0 state with the $R[\text{H}^-]$ configuration or the H^+ state with the $R[\text{H}^0]$ configuration, and so on. Thus DMC seems to increase the estimations of transition barriers. This behavior is consistent with a general drawback of GGA. Semilocal functionals of DFT are known to underestimate activation barriers of chemical reactions due to the subtle electronic structures of the transition state[71]. Because DMC can

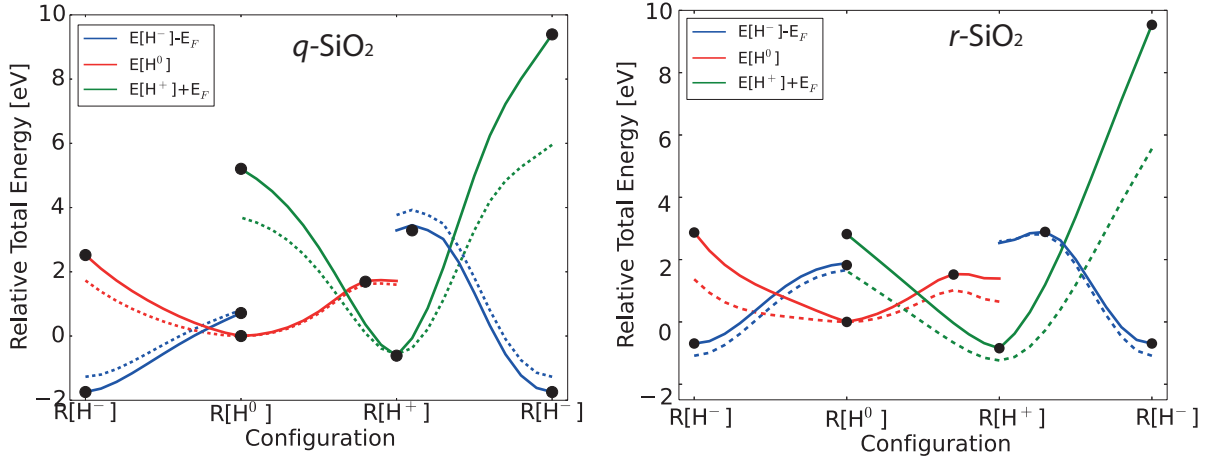


Figure 5.1: Transition barriers of hydrogen impurity in q -SiO₂ (left) and in r -SiO₂ (right). The dashed line is the PES calculated with DFT-GGA and the solid line is with DMC.

retrieve electron correlation with high accuracy, the error in GGA can be corrected with DMC. The underestimation with GGA and the correction with DMC are also known to occur in an activation barrier of the diffusion of an impurity in solids[28]. In the same way as chemical reactions without a change of charge state, GGA seems to underestimate the transition barriers between different charge states. Therefore accurate DMC seems to predict the higher transition barriers than GGA.

Figure. 5.2 and 5.3 illustrate the dependence of calculated transition barriers on the Fermi energy. The range of the Fermi energy is between VBM and CBM calculated with each method. Decreasing the Fermi energy reduces the transition barrier from H⁰ to H⁺ and H⁻ to H⁰, and increasing the Fermi energy reduces the transition barrier from H⁰ to H⁻ and H⁺ to H⁰. In the shaded region, the H⁰ state has finite barriers for transitions to H⁺ and H⁻ and therefore is metastable. When the Fermi energy takes the value outside the shaded region, H⁰ is not even metastable and therefore will change its charge state to H⁺ or H⁻ corresponding to the Fermi energy. Note that this transition barrier corresponds to a situation where electrons or holes on the Fermi level are around the defect. Because the actual reaction path is, of course, more complicated than ours, the calculated transition barrier is the upper bound of the actual ones. The transition barriers calculated with the optimized reaction path is discussed in the next section.

In q -SiO₂, there are upper and lower bound of the Fermi energy where the H⁰ state is metastable, and this trend is common to both PBE and DMC. This indicates that, in n-type or p-type q -SiO₂, the H⁰ state is not even metastable and translate into the H⁻ or H⁺ state. By contrast, the H⁰ state in r -SiO₂ has finite transition barrier even when the Fermi energy is at the conduction band minimum. Therefore, isolated hydrogen atom can

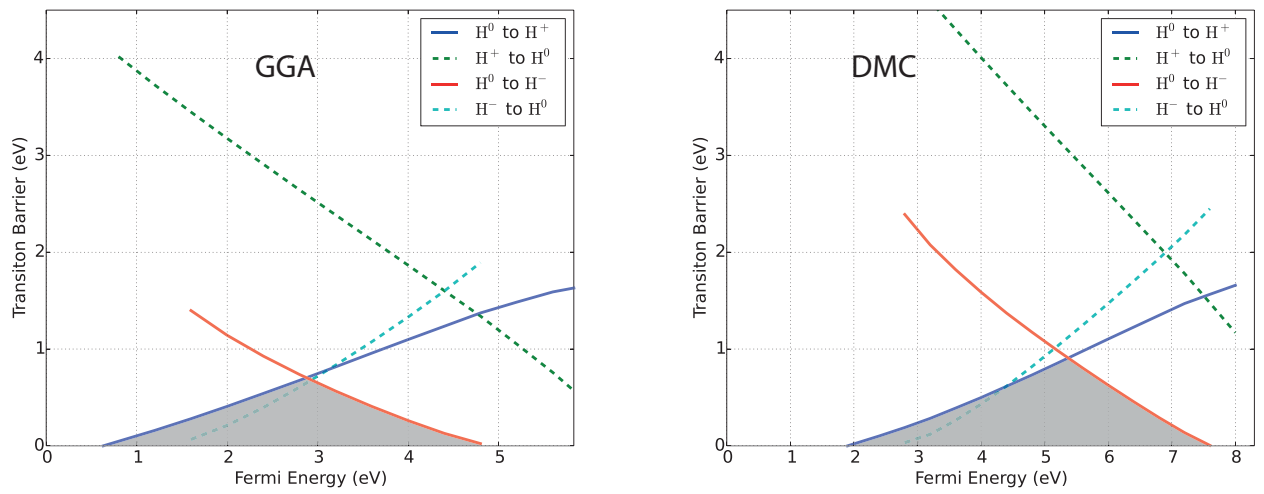


Figure 5.2: Dependence of transition barriers on the Fermi energy in q -SiO₂ calculated with linearly interpolated reaction paths.

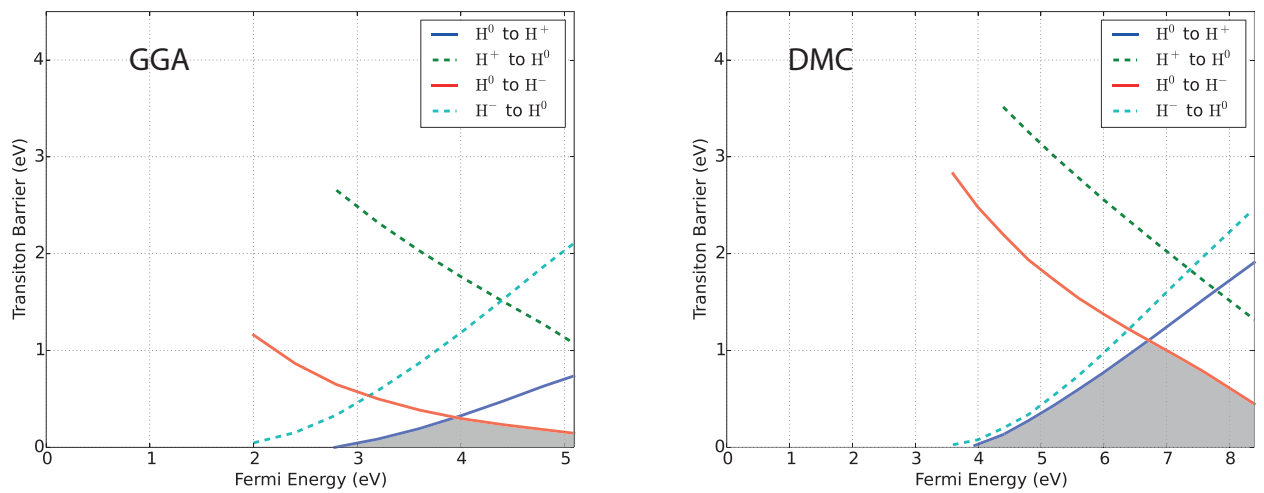


Figure 5.3: Dependence of transition barriers on the Fermi energy in r -SiO₂. calculated with linearly interpolated reaction paths.

exist metastably in n-type r -SiO₂.

We note a relation between the transition barriers and μ SR experiments[13, 14]. In the μ SR experiments, majority of incident muons becomes muonium (Mu⁰), which is a counterpart of H⁰. However, as discussed in the previous chapter, H⁰ or Mu⁰ is not thermodynamically stable. Although the reason why majority of the muons becomes Mu⁰ is still unresolved, the existence of Mu⁰ can be explained by the finite transition barriers between neutral and other charge states existing in some regions of the Fermi energy. Furthermore, the calculated barriers suggest that muonium is metastable in n-type r -SiO₂ but not even metastable in n-type q -SiO₂. Therefore, the results predict that no muonium seems to be found in n-type q -SiO₂.

We compared the calculated barriers with a temperature dependence of experimental ESR signals of H⁰. Because the temperature dependence of ESR signals in q -SiO₂ or in r -SiO₂ is not found, we use the dependence in amorphous SiO₂ (a -SiO₂)[11]. Both q -SiO₂ and a -SiO₂ have tetrahedrally coordinated SiO₂, and we expect that both systems have similar transition barriers. In the experiment, H⁰ is produced by irradiation and the population decreases with increasing the annealing temperature. The decrease may be due to the reactions such as H⁰ \rightarrow H^{+/-} or 2H⁰ \rightarrow H₂. Among these reactions, we only take the H⁰ \rightarrow H^{+/-} reaction into account. From the temperature dependence of experimental ESR populations, the activation barrier is estimated as about 0.51 eV. On the other hand, our results (Fig. 5.2) indicate that the barriers between H⁰ and H^{+/-} take the values from 0 eV to 0.91 eV. Our calculated barriers thus seem to be consistent with the experimental barriers.

5.2 Reaction path with the extended nudged elastic band method

We optimized the reaction path between different charge states with the extended NEB method developed in this study(Sec. 3.2). The calculations were performed with DFT-PBE with the computational conditions written in section 4.1.1. The number of atoms were 73 both for q -SiO₂ and r -SiO₂. We took 11 images to represent a path. The spring constant for the NEB method was optimized with smaller cell calculations (13 atoms) of r -SiO₂, and the optimized one is 0.2 Hartree/Bohr². This value was also used for q -SiO₂. The images were relaxed until residual NEB forces were below 2×10^{-3} Hartree/Bohr.

The calculated transition barriers between H⁰ and other charge states for q -SiO₂ are illustrated in Fig. 5.4. The Fermi energy was taken as 2.88 eV above the VBM where the transition barrier of H⁰ to H⁻ and H⁰ to H⁺ take the same value with a straight reaction path (the Fermi energy of the cross point of red and blue lines in Fig.5.2). By optimizing the reaction path, the calculated transition barriers reduce their values about several tenth

of an eV. However, even with the extended NEB method, the finite transition barriers still exists. Therefore, the barrier indicates that H^0 is metastable in some regions of the Fermi energy.

Figure 5.5 illustrates the transition barriers for r -SiO₂ calculated with the extended NEB method. The Fermi energy was taken as 3.95 eV above the VBM, which is the equivalent setting as for q -SiO₂ in the previous paragraph. Same as q -SiO₂, the optimized paths lower the calculated transition barriers about several tenth of an eV than the straight path. The calculated transition barrier from $H^0 \rightarrow H^-$ is very small and easily activated. This indicates that there is no transition barrier for the reaction. However, because DMC largely increases the calculated transition barriers as shown in the previous section, there may be a finite barrier for that reaction with DMC. It is an important future work to estimate the transition barriers with the extended NEB method and DMC.

In both q -SiO₂ and r -SiO₂, the transition barriers with the optimized path are several tenth of an eV lower than that with the linear path. This amount of reduction seems to be typical when the extended NEB method is used. The reduction is large enough to affect the predictions of the stability of charge states and diffusion process of hydrogen. Therefore the extended NEB method developed in this study is essential to estimate the barriers.

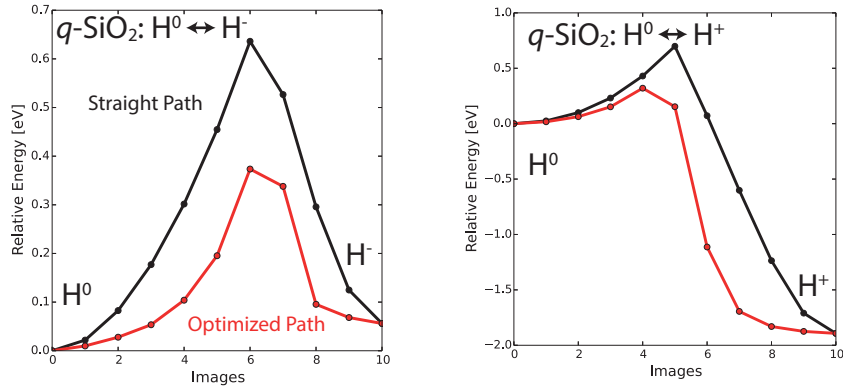


Figure 5.4: Transition barriers between H⁰ and H⁻ (left) and that between H⁰ and H⁺ (right) in q -SiO₂ with a straight path and a path optimized with the extended NEB method. The Fermi energy is taken as 2.88 eV above the VBM.

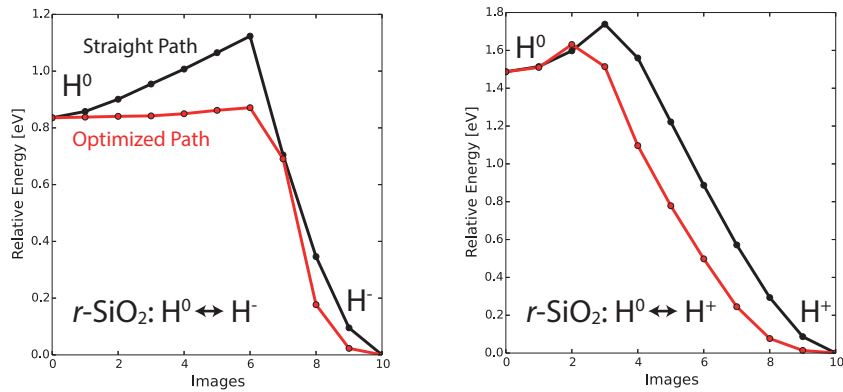


Figure 5.5: Transition barriers between H⁰ and H⁻ (left) and that between H⁰ and H⁺ (right) in r -SiO₂ with a straight path and a path optimized with the extended NEB method. The Fermi energy is taken as 3.95 eV above the VBM.

Chapter 6

Hydrogen molecules in silica

Hydrogen molecules in solids are called the hidden hydrogen reservoir because they are not detectable with infrared spectroscopy and are sometimes missed in experiments. A typical example is H_2 molecules in ZnO. Annealing the sample produces an additional O-H vibrational mode in spite of no H-related modes present before annealing. The additional mode is formed by supplying hydrogens from the hidden hydrogen reservoir, the H_2 molecules.

Hydrogen molecules are known to be beneficial in an optical lenses for photolithography, as described in 1.2. Hydrogen molecules in silica are also studied from the earth-science interests. Silica is abundant in earth's crust or mantle and undergoes the pressure-induced phase transition towards various types of polymorphs. Besides silica, high-pressure gases are known to exist in the crust and mantle. Therefore, small molecules such as H_2 or He may penetrate into silicas and may affect their physical properties, such as the compressibility.

In this section, we study stable forms of molecular hydrogen complexes in $q\text{-SiO}_2$ and $r\text{-SiO}_2$ and their thermodynamical stability. We also estimate vibrational frequencies of the hydrogen molecules, which are detectable with the Raman spectroscopy.

6.1 Atomic configurations of molecular hydrogen complexes

We optimized the atomic configurations of two interstitial hydrogens in $q\text{-SiO}_2$ and $r\text{-SiO}_2$ with DFT using the PBE functional. Computational conditions were the same as in Sec. 4.1.1. Figure 6.1 and 6.2 show the optimized structures with a neutral charge state. For $q\text{-SiO}_2$, we find that there are two kinds of stable structures, a H_2 molecule and a H_2^* complex. The H_2 molecule in $q\text{-SiO}_2$ has a bond length of 0.745 Å, which is close to the value of a free H_2 molecule 0.753 Å in PBE calculation. The H_2^* structure is a complex of H^+ and H^- impurities, where H^+ and H^- are located in a nearest neighbor site. This

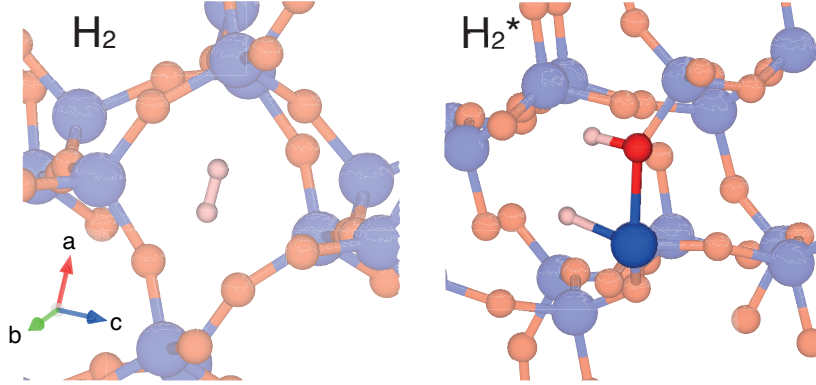


Figure 6.1: The optimized structures of complexes of two hydrogen impurities in q -SiO₂. Left figure illustrates the structure of a H₂ molecule and right a H₂^{*} complex.

structure is more stable than the structure with separated H⁺ and H⁻ impurities.

For r -SiO₂, we found two stable forms of molecular hydrogen, one of which is oriented along c -axis (labeled H₂(c)) and another one is located in ab -plane (H₂(ab)) (Fig. 6.2). The bond lengths are 0.708 Å and 0.692 Å in H₂(c) and H₂(ab), respectively. The energy of H₂ state is lower than H⁺ + H⁻ impurities about 2.94 eV and 2.67 eV for H₂(c) and H₂(ab), respectively, with PBE calculation. With DMC, the calculated energy difference between H₂ and H⁺ + H⁻ is 3.8(2) eV for H₂(ab) and 4.2(2) eV for H₂(c).

Figure 6.3 shows DOS and PDOS of hydrogen for H₂ in q -SiO₂ and r -SiO₂. In r -SiO₂, there is an in-gap state assigned to hydrogen whereas no in-gap state appears in q -SiO₂. This indicates the possible existence of the H₂⁺ state in r -SiO₂. This difference between q -SiO₂ and r -SiO₂ may be due to a hybridization of H₂ orbitals with the host crystal. Because the interstitial spacing is smaller in r -SiO₂ than in q -SiO₂, the hybridization is stronger in r -SiO₂ and the in-gap state appears.

The atomic configurations of the H₂⁺ state in r -SiO₂ are shown in Fig. 6.4. In this state, an electron is removed from the H₂ molecule, and the remaining electron is located at the H₂⁺ molecule. For q -SiO₂, if we remove an electron from the system, the electron gets out of host SiO₂. Thus H₂⁺ state does not exist in q -SiO₂ and is unique in r -SiO₂. The H₂⁺ state has two stable geometries, H₂⁺(c) and H₂⁺(ab) similar to H₂ state. The bond lengths of H₂⁺(c) and H₂⁺(ab) are 0.843 Å and 0.861 Å, respectively, which is longer than the bond lengths of the H₂ states. The orientation of a H₂ molecule is different between in the H₂ state and in the H₂⁺ state. In the H₂ state, the molecule is directed to avoid surrounding oxygen atoms and causes a large lattice relaxation. On the other hand, in the H₂⁺ state, the molecule turns and directed towards the oxygen atoms with the host lattice almost unchanged.

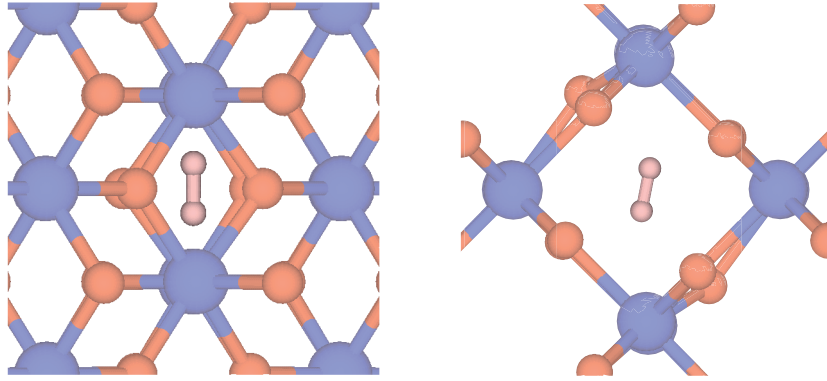


Figure 6.2: The optimized structures of complexes of two hydrogen impurities in r -SiO₂. Left figure illustrates the structure of a H₂ molecule oriented to c -axis and right locates in ab -plane.

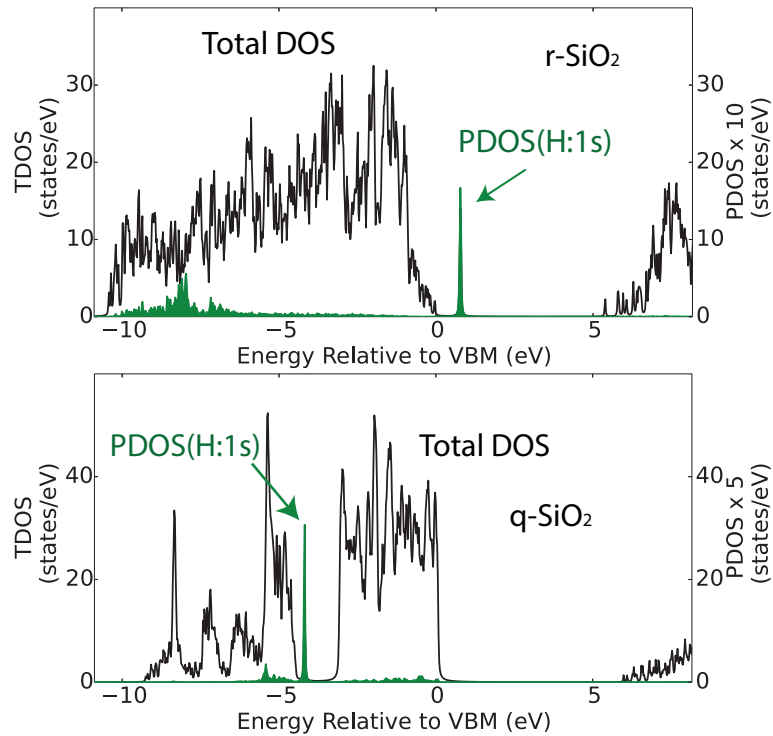


Figure 6.3: Density of states and partial density of states of H₂ in q -SiO₂ and r -SiO₂ calculated with Si₂₄O₄₈H₂ structures. The upper panel corresponds to r -SiO₂ and the lower panel to q -SiO₂. In each panel, total DOS is shown in black lines and PDOS of H in green line.

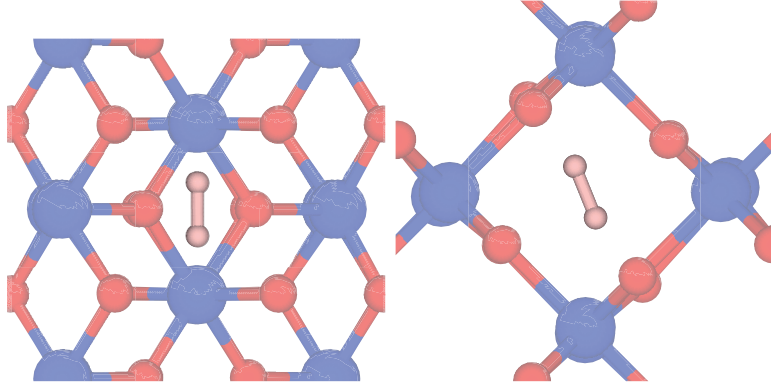


Figure 6.4: The optimized structures of H_2^+ impurities with different configurations. Left: H_2^+ oriented along c-axis. Right: H_2^+ located in ab-plane.

6.2 Formation energy of molecular hydrogen complex

We evaluated the formation energies of molecular hydrogen complexes in order to determine the thermodynamically stable states (Fig. 6.5). The calculated formation energies with GGA and DMC are plotted in the regions of the Fermi energy between VBM and CBM calculated with each method. The origin of the Fermi energy is taken as VBM calculated with DMC. Figure 6.5 shows not only the formation energies of hydrogen complexes discussed in the previous section but also that of two separated hydrogen impurities such as $2\text{H}^+ = \text{H}^+ + \text{H}^+$. In q - SiO_2 , as a two-hydrogen impurity, 2H^+ , 2H^- and the H_2 molecule are thermodynamically stable. Although $\text{H}^+ + \text{H}^-$ is the most stable in two mono-hydrogen impurities, H_2 molecule is more stable than this state. H_2^* state has higher energy than H_2 molecule, and therefore not thermodynamically stable. However, H_2^* may affect the diffusion mechanism of hydrogen impurity. When hydrogen atom diffuses through the interstitial voids of q - SiO_2 with rich hydrogen impurities, the atom may hop between the H_2^* states.

In r - SiO_2 , only $\text{H}^+ + \text{H}^+$ and $\text{H}_2(\text{c})$ molecule is thermodynamically stable. Other states such as $\text{H}^- + \text{H}^-$ or the H_2^+ state are not thermodynamically stable. Although H_2^+ state is metastable, it may be created by irradiation and detected with ESR experiments.

Both in q - SiO_2 and r - SiO_2 , H_2 molecule is thermodynamically stable. Therefore, H_2 molecules may exist in both systems as a hidden hydrogen reservoir.

6.3 Vibrational frequencies of hydrogen molecules in silica

We calculated the vibrational frequencies of hydrogen molecules in silica with the PBE functional in order to access the experimental identification of the molecules. We estimated

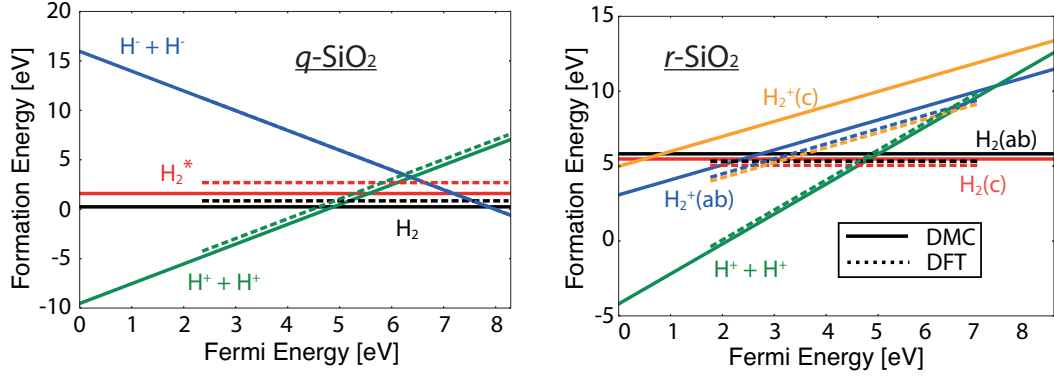


Figure 6.5: The formation energies of molecular hydrogen complexes in q -SiO₂ (left) and in r -SiO₂ (right).

the vibrational frequencies with changing the bond length of H₂ molecules whereas fixing the structure of the host lattice. Calculated frequencies for neutral H₂ molecules are 4318.12 cm⁻¹ for a free H₂, 4390.31 cm⁻¹ for H₂ in q -SiO₂, 4834.26 cm⁻¹ and 5166.30 cm⁻¹ for H₂(c) and H₂(ab) in r -SiO₂, respectively. The frequencies for H₂⁺ are 2820.62 cm⁻¹ in vacuum, 3066.67 cm⁻¹ and 4149.86 cm⁻¹ for H₂⁺(c) and H₂⁺(ab) in r -SiO₂, respectively. These frequencies are well separated and can be distinguished with spectroscopy. These vibrational frequencies may be observable by the Raman scattering technique.

Chapter 7

Conclusions

In this thesis, we investigated the properties of hydrogen impurities in silica with reliable first-principles methods. Generally, hydrogen impurity in semiconductors can adopt multiple charge states due to the amphoteric character of the hydrogen atom. The relative stability between these states is known to be quite subtle, which have rendered reliable investigation on them difficult. We have addressed this problem with efficient first-principles methods. Specifically, we employed the diffusion Monte Carlo (DMC) method to achieve reliable description of electronic structures. Also, we developed a method to calculate the energy barriers between different charge states by extending the nudged elastic band (NEB) method. Applying these methods to silica, we have achieved precise description of the possible hydrogen charge states there.

In chapter 3, we showed the extension of the NEB method, which enables us to calculate the minimum energy path across the potential energy surfaces for different charge states.

In chapter 4, we studied the properties of single hydrogen impurity in quartz SiO_2 ($q\text{-SiO}_2$) and rutile SiO_2 ($r\text{-SiO}_2$) with a combined analysis based on the first-principles method based on density functional theory (DFT) and the DMC. We calculated the formation energies of hydrogen for three possible charge states (H^- , H^0 , H^+) and find that the formation energy for the H^0 state is larger than those for H^+ and H^- , which is consistent with the DFT and DMC approaches. This result indicates that hydrogen impurity is amphoteric and isolated hydrogen H^0 is not thermodynamically stable. There is quantitative difference between DFT and DMC. Compared to DFT, calculated formation energies with DMC are lower for H^+ in $q\text{-SiO}_2$ and higher for H^- in $r\text{-SiO}_2$ whereas other states are unchanged. These results indicate that the effect of electronic correlation, which is accurately treated with the DMC, may be particularly large for these states. The origin of this may be due to the difference in electronic structures of the systems arose from different coordination number. The fact that DFT and DMC give different formation energies indicates the importance to use reliable first-principles methods to describe electronic structures of

hydrogen-related systems.

In chapter 5, we estimate transition barriers between different charge states with a new method described in chapter 3. The calculated barriers indicate that each charge state is stable in some regions of the electronic chemical potential and is not even metastable in other regions. For n-type or p-type q -SiO₂, isolated hydrogen is not metastable. This indicates that during the diffusion in n-type and p-type q -SiO₂, hydrogen atom does not adopt the H⁰ state. Comparing the barriers calculated with DFT and DMC, DMC gives larger values in both q -SiO₂ and r -SiO₂, and so this behavior may be general. We compared the barriers obtained with the simple straight paths and that obtained with the minimum energy path calculated with the extended NEB method. The result indicates that the calculated barriers are lower with the NEB method about several tenth of an eV, which is large enough to affect the predictions of the stability of charge states and diffusion process of hydrogen. Therefore the new NEB method developed in this study is essential to describe the transition barriers between different charge states.

In chapter 6, we studied the possible forms of molecular complexes of two hydrogen atoms and their stability. In q -SiO₂, we found two stable forms, hydrogen molecule (H₂) and H₂^{*} complex. The latter is a complex of nearest-neighbored H⁺ and H⁻. For r -SiO₂, we found two stable forms, H₂ and H₂⁺. Uniquely, the H₂⁺ molecule is stabilized only in r -SiO₂. This is due to the interactions between H₂ molecule and host SiO₂. Because interstitial voids of r -SiO₂ is smaller than that of q -SiO₂, H₂ in r -SiO₂ has larger interactions with host SiO₂. This may be the reason why H₂⁺ is stable in r -SiO₂. As two hydrogen impurities, thermodynamically stable states in q -SiO₂ are H⁺ + H⁺, H₂ and H⁻ + H⁻. The H₂^{*} state is metastable in q -SiO₂, but this state may be still important to discuss the diffusion process of hydrogen atoms. In r -SiO₂, H⁺ + H⁺ and H₂ are thermodynamically stable whereas H₂⁺ is metastable, but the H₂⁺ state is nevertheless important because this state is detectable with electron spin resonance experiments of an irradiated sample.

We conclude this thesis by future perspectives around this work. Assessing the reliability of DFT to describe systems including hydrogens is important to study hydrogen-related technologies, such as hydrogen storage or fuel cell. This study shows that, even in weakly correlated systems, DFT may give different predictions from DMC. This fact suggests the importance to use accurate first-principles methods to study hydrogen systems. Because the total energy is not feasible in the perturbative methods, such as the GW method, some of wave function theories, such as DMC, is a promising one as shown in this study. Furthermore, DMC is suitable for massively parallel computations. We therefore expect future applications of DMC to hydrogen systems.

The method to calculate transition barriers between different charge states may have various possible applications. A typical one is to study the diffusion process of impurities. Hydrogen impurity adopts several charge states in various semiconductors. Furthermore,

not only hydrogen but also many other impurities have several stable charge states. When the impurities diffuse in solids, they may exchange electrons with other defects and thus can change its charge state during the diffusion. To treat such a diffusion, the transition barriers between different states are fundamental information.

Acknowledgements

I would like to express my greatest and heartfelt appreciation towards my supervisor Professor Shinji Tsuneyuki. His continuous and sincere encouragements helped me to overcome many crisis situations. Without him, this dissertation would never have been possible. I would also like to offer special thanks to Assistant Professor Ryosuke Akashi. His insightful comments gave me better understanding of my research field.

I am indebted to all the members of Tsuneyuki Research Group. Discussions with them were exciting and helped me improve my understanding of condensed matter physics in wide area. I also express my gratitude to secretary Emi Shimosikiryo for her constant support. Her practical advice about diet enhanced my vitality, which is necessary to achieve this work. I also thank to ex-members of Tsuneyuki Research Group. Especially, I owe a very important debt to Assistant Professor Masayuki Ochi for his encouragement and fruitful discussions.

The computations in this work were performed using the facilities of the Supercomputer Center, the Institute for Solid State Physics, the University of Tokyo, and the facilities of the Supercomputing Division, Information Technology Center, the University of Tokyo.

Last but not least, I would like to thank my mother and brother for their long-term support.

Bibliography

- [1] C. G. Van de Walle and J. Neugebauer, “Hydrogen in semiconductors,” *Annu. Rev. Mater. Res.* **36**, 179 (2006).
- [2] S. Iimura, S. Matsuishi, H. Sato, T. Hanna, Y. Muraba, S. W. Kim, J. E. Kim, M. Takata, and H. Hosono, “Two-dome structure in electron-doped iron arsenide superconductors.” *Nat. Commun.* **3**, 943 (2012).
- [3] A. P. Drozdov, M. I. Eremets, I. A. Troyan, V. Ksenofontov, and S. I. Shylin, “Conventional superconductivity at 203 kelvin at high pressures in the sulfur hydride system.” *Nature* **525**, 73 (2015).
- [4] S. F. J. Cox, J. S. Lord, S. P. Cottrell, J. M. Gil, H. V. Alberto, A. Keren, D. Prabhakaran, R. Scheuermann, and A. Stoykov, “Oxide muonics: I. Modelling the electrical activity of hydrogen in semiconducting oxides,” *J. Phys. Condens. Matter* **18**, 1061 (2006).
- [5] S. F. J. Cox, J. L. Gavartin, J. S. Lord, S. P. Cottrell, J. M. Gil, H. V. Alberto, J. P. Duarte, R. C. Vilão, N. A. d. Campos, D. J. Keeble, E. A. Davis, M. Charlton, and D. P. v. d. Werf, “Oxide muonics: II. Modelling the electrical activity of hydrogen in wide-gap and high-permittivity dielectrics,” *J. Phys. Condens. Matter* **18**, 1079 (2006).
- [6] S. F. J. Cox, “Muonium as a model for interstitial hydrogen in the semiconducting and semimetallic elements,” *Rep. Prog. Phys.* **72**, 116501 (2009).
- [7] S. K. Estreicher, “Hydrogen-related defects in crystalline semiconductors: a theorist’s perspective,” *Mater. Sci. Eng. R-Rep.* **14**, 319 (1995).
- [8] P. Hohenberg and W. Kohn, “Inhomogeneous electron gas,” *Phys. Rev.* **136**, B864 (1964).
- [9] W. Kohn and L. J. Sham, “Self-consistent equations including exchange and correlation effects,” *Phys. Rev.* **140**, A1133 (1965).

- [10] B. D. Perlson and J. A. Weil, "Atomic hydrogen in α -quartz," *J. Magn. Reson.* **15**, 594 (1974).
- [11] D. L. Griscom, M. Stapelbroek, and E. J. Friebele, "ESR studies of damage processes in X-irradiated high purity α -SiO₂:OH and characterization of the formyl radical defect," *J. Chem. Phys.* **78**, 1638 (1983).
- [12] T. Miyazaki, N. Azuma, S. Yoshida, and K. Fueki, "Comparison of long-range activation transfer in gamma-radiolysis of single crystalline quartz with amorphous silica," *Int. J. Radiat. Appl. Instrum. C Radiat. Phys. Chem.* **32**, 695 (1988).
- [13] G. G. Myasishcheva, Y. V. Obukhov, V. S. Roganov, and V. G. Firsov, "A search for atomic muonium in chemically inert substances," *Sov. Phys. JETP* **26**, 298 (1968).
- [14] N. Funamori, K. M. Kojima, D. Wakabayashi, T. Sato, T. Taniguchi, N. Nishiyama, T. Irifune, D. Tomono, T. Matsuzaki, M. Miyazaki, M. Hiraishi, A. Koda, and R. Kadono, "Muonium in Stishovite: Implications for the Possible Existence of Neutral Atomic Hydrogen in the Earth's Deep Mantle," *Sci. Rep.* **5**, 8437 (2015).
- [15] A. Yokozawa and Y. Miyamoto, "First-principles calculations for charged states of hydrogen atoms in SiO₂," *Phys. Rev. B* **55**, 13783 (1997).
- [16] P. E. Blöchl, "First-principles calculations of defects in oxygen-deficient silica exposed to hydrogen," *Phys. Rev. B* **62**, 6158 (2000).
- [17] J. Godet and A. Pasquarello, "*Ab initio* study of charged states of H in amorphous SiO₂," *Microelectron. Eng.* **80**, 288 (2005).
- [18] B. Tuttle, "Energetics and diffusion of hydrogen in SiO₂," *Phys. Rev. B* **61**, 4417 (2000).
- [19] J. Godet and A. Pasquarello, "Proton diffusion mechanism in amorphous SiO₂," *Phys. Rev. Lett.* **97**, 155901 (2006).
- [20] J. A. Santana, J. T. Krogel, J. Kim, P. R. C. Kent, and F. A. Reboredo, "Structural stability and defect energetics of ZnO from diffusion quantum Monte Carlo," *J. Chem. Phys.* **142**, 164705 (2015).
- [21] G. Henkelman and H. Jónsson, "Improved tangent estimate in the nudged elastic band method for finding minimum energy paths and saddle points," *J. Chem. Phys.* **113**, 9978 (2000).
- [22] W. M. C. Foulkes, L. Mitas, R. J. Needs, and G. Rajagopal, "Quantum Monte Carlo simulations of solids," *Rev. Mod. Phys.* **73**, 33 (2001).

-
- [23] R. J. Needs, M. D. Towler, N. D. Drummond, and P. López Ríos, “Continuum variational and diffusion quantum Monte Carlo calculations,” *J. Phys. Condens. Matter* **22**, 023201 (2010).
- [24] J. Kolorenč and L. Mitas, “Applications of quantum Monte Carlo methods in condensed systems,” *Rep. Prog. Phys.* **74**, 026502 (2011).
- [25] H. Zheng and L. K. Wagner, “Computation of the correlated metal-insulator transition in vanadium dioxide from first principles,” *Phys. Rev. Lett.* **114**, 176401 (2015).
- [26] L. K. Wagner, “Ground state of doped cuprates from first-principles quantum Monte Carlo calculations,” *Phys. Rev. B* **92**, 161116(R) (2015).
- [27] A. Benali, L. Shulenburger, N. A. Romero, J. Kim, and O. A. von Lilienfeld, “Application of diffusion Monte Carlo to materials dominated by van der Waals interactions,” *J. Chem. Theory Comput.* **10**, 3417 (2014).
- [28] W. K. Leung, R. J. Needs, G. Rajagopal, S. Itoh, and S. Ihara, “Calculations of silicon self-interstitial defects,” *Phys. Rev. Lett.* **83**, 2351 (1999).
- [29] R. Q. Hood, P. R. C. Kent, R. Needs, and P. R. Briddon, “Quantum Monte Carlo study of the optical and diffusive properties of the vacancy defect in diamond,” *Phys. Rev. Lett.* **91**, 076403 (2003).
- [30] R. Q. Hood, P. R. C. Kent, and F. A. Reboredo, “Diffusion quantum Monte Carlo study of the equation of state and point defects in aluminum,” *Phys. Rev. B* **85**, 134109 (2012).
- [31] D. Alfè and M. Gillan, “Schottky defect formation energy in MgO calculated by diffusion Monte Carlo,” *Phys. Rev. B* **71**, 220101(R) (2005).
- [32] R. G. Parr and W. Yang, “Density-functional theory of atoms and molecules,” (Oxford University Press, 1989).
- [33] J. P. Perdew and A. Zunger, “Self-interaction correction to density-functional approximations for many-electron systems,” *Phys. Rev. B* **23**, 5048 (1981).
- [34] J. P. Perdew, K. Burke, and M. Ernzerhof, “Generalized gradient approximation made simple,” *Phys. Rev. Lett.* **77**, 3865 (1996).
- [35] D. M. Ceperley and B. J. Alder, “Ground state of the electron gas by a stochastic method,” *Phys. Rev. Lett.* **45**, 566 (1980).

- [36] P. Mori-Sánchez, A. J. Cohen, and W. Yang, “Localization and delocalization errors in density functional theory and implications for band-gap prediction.” *Phys. Rev. Lett.* **100**, 146401 (2008).
- [37] J. Heyd, G. E. Scuseria, and M. Ernzerhof, “Hybrid functionals based on a screened coulomb potential,” *J. Chem. Phys.* **118**, 8207 (2003).
- [38] N. D. Drummond, M. D. Towler, and R. J. Needs, “Jastrow correlation factor for atoms, molecules, and solids,” *Phys. Rev. B* **70**, 235119 (2004).
- [39] T. Kato, “On the eigenfunctions of many-particle systems in quantum mechanics,” *Comm. Pure Appl. Math.* **10**, 151 (1957).
- [40] N. D. Drummond and R. J. Needs, “Variance-minimization scheme for optimizing Jastrow factors,” *Phys. Rev. B* **72**, 085124 (2005).
- [41] J. B. Anderson, “A random-walk simulation of the Schrödinger equation: H_3^+ ,” *J. Chem. Phys.* **63**, 1499 (1975).
- [42] J. B. Anderson, “Quantum chemistry by random walk. $H\ ^2P$, $H_3^+ D_{3h}\ ^1A_1$, $H_2\ ^3\Sigma_u^+$, $H_4\ ^1\Sigma_g^+$, $Be\ ^1S$,” *J. Chem. Phys.* **65**, 4121 (1976).
- [43] L. Hedin, “New method for calculating the one-particle green’s function with application to the electron-gas problem,” *Phys. Rev.* **139**, A796 (1965).
- [44] F. Aryasetiawan and O. Gunnarsson, “The gw method,” *Rep. Prog. Phys.* **61**, 237 (1998).
- [45] M. Shishkin, M. Marsman, and G. Kresse, “Accurate quasiparticle spectra from self-consistent gw calculations with vertex corrections,” *Phys. Rev. Lett.* **99**, 246403 (2007).
- [46] G. H. Booth, A. Grüneis, G. Kresse, and A. Alavi, “Towards an exact description of electronic wavefunctions in real solids,” *Nature* **493**, 365–70 (2013).
- [47] G. Makov and M. C. Payne, “Periodic boundary conditions in *ab initio* calculations,” *Phys. Rev. B* **51**, 4014 (1995).
- [48] Y. Kumagai and F. Oba, “Electrostatics-based finite-size corrections for first-principles point defect calculations,” *Phys. Rev. B* **89**, 195205 (2014).
- [49] C. Freysoldt, B. Grabowski, T. Hickel, J. Neugebauer, G. Kresse, A. Janotti, and C. G. Van de Walle, “First-principles calculations for point defects in solids,” *Rev. of Mod. Phys.* **86**, 253 (2014).

-
- [50] G. Henkelman, B. P. Uberuaga, and H. Jónsson, “A climbing image nudged elastic band method for finding saddle points and minimum energy paths,” *J. Chem. Phys.* **113**, 9901 (2000).
- [51] Y. Xu and M. Mavrikakis, “Adsorption and dissociation of O₂ on gold surfaces: effect of steps and strain,” *J. Phys. Chem. B* **107**, 9298–9307 (2003).
- [52] D. E. Jiang and E. A. Carter, “Diffusion of interstitial hydrogen into and through bcc Fe from first principles,” *Phys. Rev. B* **70** (2004).
- [53] M. G. Wardle, J. P. Goss, and P. R. Briddon, “First-principles study of the diffusion of hydrogen in ZnO,” *Phys. Rev. Lett.* **96**, 205504 (2006).
- [54] D. Sheppard, R. Terrell, and G. Henkelman, “Optimization methods for finding minimum energy paths,” *J. Chem. Phys.* **128**, 134106 (2008).
- [55] J. Yamauchi, M. Tsukada, S. Watanabe, and O. Sugino, “First-principles study on energetics of c-BN(001) reconstructed surfaces,” *Phys. Rev. B* **54**, 5586 (1996).
- [56] O. Sugino and A. Oshiyama, “Vacancy in Si: Successful description within the local-density approximation,” *Phys. Rev. Lett.* **68**, 1858 (1992).
- [57] M. Bernasconi, G. L. Chiarotti, P. Focher, S. Scandolo, E. Tosatti, and M. Parrinello, “First-principle-constant pressure molecular dynamics,” *J. Phys. Chem. Solids* **56**, 501 (1995).
- [58] D. Alfè and M. Gillan, “Efficient localized basis set for quantum Monte Carlo calculations on condensed matter,” *Phys. Rev. B* **70**, 161101(R) (2004).
- [59] A. Szabo and N. S. Ostlund, *Modern Quantum Chemistry: Introduction to Advanced Electronic Structure Theory*, Dover Books on Chemistry Series (Dover Publications, 1996).
- [60] J. P. Perdew, M. Ernzerhof, and K. Burke, “Rationale for mixing exact exchange with density functional approximations,” *J. Chem. Phys.* **105**, 9982 (1996).
- [61] P. López Ríos, A. Ma, N. D. Drummond, M. D. Towler, and R. J. Needs, “Inhomogeneous backflow transformations in quantum Monte Carlo calculations,” *Phys. Rev. E* **74**, 066701 (2006).
- [62] M. Bajdich, L. Mitás, G. Drobný, L. K. Wagner, and K. E. Schmidt, “Pfaffian pairing wave functions in electronic-structure quantum Monte Carlo simulations.” *Phys Rev Lett* **96**, 130201 (2006).

- [63] L. Mitás, E. L. Shirley, and D. M. Ceperley, “Nonlocal pseudopotentials and diffusion Monte Carlo,” *J. Chem. Phys.* **95**, 3467 (1991).
- [64] M. Casula, “Beyond the locality approximation in the standard diffusion Monte Carlo method,” *Phys. Rev. B* **74**, 161102(R) (2006).
- [65] U. Itoh, “Vacuum ultraviolet absorption cross sections of SiH_4 , GeH_4 , Si_2H_6 , and Si_3H_8 ,” *J. Chem. Phys.* **85**, 4867 (1986).
- [66] W. Meyer, “Ionization energies of water from PNO-CI calculations,” *Int. J. Quant. Chem.* **5**, 341 (1971).
- [67] C. Lin, F. H. Zong, and D. M. Ceperley, “Twist-averaged boundary conditions in continuum quantum Monte Carlo algorithms,” *Phys. Rev. E* **64**, 016702 (2001).
- [68] A. Badinski, P. D. Haynes, J. R. Trail, and R. J. Needs, “Methods for calculating forces within quantum Monte Carlo simulations.” *J. Phys. Condens. Matter* **22**, 074202 (2010).
- [69] K. E. Riley, B. T. Op’t Holt, and K. M. Merz, “Critical assessment of the performance of density functional methods for several atomic and molecular properties,” *J. Chem. Theory Comput.* **3**, 407 (2007).
- [70] T. Miyake, T. Ogitsu, and S. Tsuneyuki, “Quantum distributions of muonium and hydrogen in crystalline silicon,” *Phys. Rev. Lett.* **81**, 1873 (1998).
- [71] A. J. Cohen, P. Mori-Sánchez, and W. Yang, “Challenges for density functional theory,” *Chem. Rev.* **112**, 289 (2011).